



Article

Geodetic SAR for Height System Unification and Sea Level Research—Results in the Baltic Sea Test Network

Thomas Gruber ^{1,*}, Jonas Ågren ², Detlef Angermann ³, Artu Ellmann ⁴, Andreas Engfeldt ², Christoph Gisinger ⁵, Leszek Jaworski ^{6,†}, Tomasz Kur ⁶, Simo Marila ⁷, Jolanta Nastula ⁶, Faramarz Nilfouroushan ², Maaria Nordman ^{7,8}, Markku Poutanen ⁷, Timo Saari ⁷, Marius Schlaak ¹, Anna Świątek ⁶, Sander Varbla ⁴ and Ryszard Zdunek ⁶

- ¹ Astronomical and Physical Geodesy, School of Engineering and Design, Technical University of Munich (TUM), 80333 Munich, Germany; marius.schlaak@tum.de
- ² Lantmäteriet (LM), Swedish Mapping, Cadastral and Land Registration Authority, 80182 Gavle, Sweden; jonas.agren@lm.se (J.Å.); andreas.engfeldt@lm.se (A.E.); faramarz.nilfouroushan@lm.se (F.N.)
- ³ Deutsches Geodätisches Forschungsinstitut, School of Engineering and Design, Technical University of Munich (TUM), 80333 Munich, Germany; detlef.angermann@tum.de
- ⁴ School of Engineering, Tallinn University of Technology (TUT), 19086 Tallinn, Estonia; artu.ellmann@taltech.ee (A.E.); sander.varbla@taltech.ee (S.V.)
- ⁵ German Aerospace Center (DLR), Remote Sensing Technology, 82234 Weßling, Germany; christoph.gisinger@dlr.de
- ⁶ Centrum Badań Kosmicznych, Polskiej Akademii Nauk (CBK-PAN), 00-716 Warsaw, Poland; tkur@cbk.waw.pl (T.K.); nastula@cbk.waw.pl (J.N.); ana@cbk.waw.pl (A.Ś.); rysiek@cbk.waw.pl (R.Z.)
- ⁷ Finnish Geospatial Research Institute (FGI), 02430 Masala, Finland; simo.marila@maanmittauslaitos.fi (S.M.); maaria.nordman@aalto.fi (M.N.); markku.poutanen@nls.fi (M.P.); timo.saari@maanmittauslaitos.fi (T.S.)
- ⁸ School of Engineering, Aalto University (AU), 00076 Aalto, Finland
- * Correspondence: thomas.gruber@tum.de; Tel.: +49-89-28923192
- † Passed away on 22 February 2021.



Citation: Gruber, T.; Ågren, J.; Angermann, D.; Ellmann, A.; Engfeldt, A.; Gisinger, C.; Jaworski, L.; Kur, T.; Marila, S.; Nastula, J.; et al. Geodetic SAR for Height System Unification and Sea Level Research—Results in the Baltic Sea Test Network. *Remote Sens.* **2022**, *14*, 3250. <https://doi.org/10.3390/rs14143250>

Academic Editors: Xiaoxing He, Jean-Philippe Montillet, Zhao Li, Gaël Kermarrec, Rui Fernandes and Feng Zhou

Received: 18 May 2022

Accepted: 5 July 2022

Published: 6 July 2022

Publisher's Note: MDPI stays neutral with regard to jurisdictional claims in published maps and institutional affiliations.



Copyright: © 2022 by the authors. Licensee MDPI, Basel, Switzerland. This article is an open access article distributed under the terms and conditions of the Creative Commons Attribution (CC BY) license (<https://creativecommons.org/licenses/by/4.0/>).

Abstract: Coastal sea level is observed at tide gauge stations, which usually also serve as height reference stations for national networks. One of the main issues with using tide gauge data for sea level research is that only a few stations are connected to permanent GNSS stations needed to correct for vertical land motion. As a new observation technique, absolute positioning by SAR using off the shelf active radar transponders can be installed instead. SAR data for the year 2020 are collected at 12 stations in the Baltic Sea area, which are co-located to tide gauges or permanent GNSS stations. From the SAR data, 3D coordinates are estimated and jointly analyzed with GNSS data, tide gauge records and regional geoid height estimates. The obtained results are promising but also exhibit some problems related to the electronic transponders and their performance. At co-located GNSS stations, the estimated ellipsoidal heights agree in a range between about 2 and 50 cm for both observation systems. From the results, it can be identified that, most likely, variable systematic electronic instrument delays are the main reason, and that each transponder instrument needs to be calibrated individually. Nevertheless, the project provides a valuable data set, which offers the possibility of enhancing methods and procedures in order to develop a geodetic SAR positioning technique towards operability.

Keywords: height system unification; sea level; geodetic SAR positioning; GNSS; tide gauge; geoid; Sentinel-1; GOCE

1. Introduction

Monitoring sea level change in an absolute sense and enabling height system unification across countries requires an integrated observing system and the consistent combination of three types of observations. In particular, these observations are geometric heights and geoid heights at tide gauge stations and the corresponding tide gauge readings.

Consistency in this context means that reference frames and processing standards to be applied during data analyses need to be identical for all three components. This has to be carefully done as the geometric network intrinsically is defined by a set of reference station coordinates (center of figure), while gravimetric quantities as the geoid intrinsically are available in a physical reference frame, which is defined by the mass distribution of the Earth (center of mass). Another issue to be considered is vertical land motion, or more general vertical station movements, which introduces a time variable component in this observing system. This is mainly reflected in time variable geometric heights but is also apparent with smaller amplitudes in geoid height variations caused by the redistribution of the attracting masses. Therefore, such a monitoring system requires repeated or ideally continuous observations of all parameters. If all this is considered carefully, one could connect tide gauges across oceans for unifying height systems and for observing the sea level in an absolute sense with respect to a global equipotential surface. A detailed description of the components of the observing system, the scientific challenges to be addressed for combining the various observations and references to related literature is provided in our first related paper [1] and is not repeated here.

As a new observing system for geometric heights, the geodetic SAR positioning technique is applied in a test network in the Baltic Sea. For this purpose, 10 stations are equipped with active SAR transponders (also called electronic corner reflectors, ECRs) and locally tied to existing tide gauges and/or permanent GNSS stations (see Figure 1). These ECRs are capable to amplify C-Band SAR signals received from the Sentinel-1 satellites and therefore are well-defined persistent scatters to be used for geodetic positioning. All details about the individual stations and the conducted experiments are described in [1].

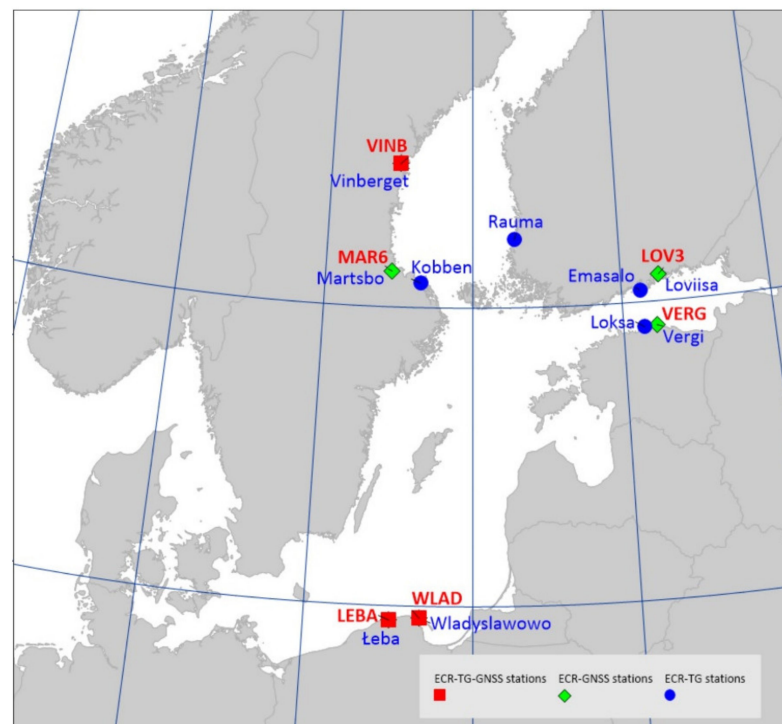


Figure 1. Baltic Sea test network showing ECR locations and ties to GNSS and/or tide gauge stations. Exact coordinates are shown in Table 4.

Data for the complete year 2020 are collected and processed in order to determine the absolute sea level at a few selected tide gauge stations in the Baltic Sea. This includes time series of GNSS and SAR observations as well as tide gauge readings. Geoid heights at the tide gauge stations are recomputed from a recent collection of terrestrial gravity data in the Baltic Sea area.

The main purpose of this paper is to summarize the processing of all observation types and to present the absolute sea level results for the chosen Baltic Sea test network. This paper complements the preliminary analyses and results described in [1] and represents the final outcome of the project including its quality assessment. First, in Section 2 and its subsections, the processing of the individual observation types and its results in terms of heights are described in detail, while in Section 3, an attempt is made to compare and combine these heights for the ultimate goal to determine absolute sea level heights and height system offsets. The paper concludes with an assessment of the results and specifically with some conclusions and recommendations about the applicability of ECRs for observing absolute sea level heights and for the connection of height systems (Section 4).

2. Data Processing and Results for Individual Observation Types

2.1. SAR Data Analysis

The aim of our Sentinel-1 SAR data analysis is to support the selection and assessment of the ECR installations sites as well as the preparation of radar timing measurements (range and azimuth) and correction files serving the SAR positioning with radargrammetric methods [1,2]. The ECR installations were performed by the different project partners in Sweden, Finland, Estonia, and Poland in 2020 in the January to June time frame. Two additional installations were performed at DLR compound in Oberpfaffenhofen, Germany, for calibration and validation purposes. The latest installation at Spikarna/Vinberget, Sweden, took place in October 2020. Logistics and obtaining the transmission licenses were the main reasons for the different installation times, which also affected operation times of the ECR network (see Table 1). The inspection of the on-site situation and careful analysis of Sentinel-1 SAR images were carried out prior to the installation in order to select locations favorable to both the contrast in the Sentinel-1 SAR images and on-ground site access. Once installed and configured, the operation proved fairly reliable with most ECRs, but three sites—Vergi (Estonia), Loviisa (Finland), and DLR2 (Oberpfaffenhofen, Germany)—experienced electronic failures, and the ECR at Loksa site (Estonia) became damaged during a severe storm event flooding the area. Therefore, only 8 out of 12 sites could be operated as planned.

Possible data acquisition with Sentinel-1 depends on the latitude, the site's location with respect to the Sentinel-1 ground track, and the coverage of the SAR instrument. The Sentinel-1 IW TOPS mode data cover a cross range of 250 km between 25° to 42° incidence angle [3], and the higher the latitude, the more overlapping tracks become available at a given site. For the mid-latitude ECR installations in Germany and Poland, this yields three to four passes within the 6-day Sentinel-1 repeat cycle, whereas the more northern sites in Finland and Sweden are covered by five to six repeat passes, see Table 1. Note that due to duty cycle limitation and data downlink constraints, Sentinel-1 does not acquire data for all available tracks over Europe, and therefore, some stations, e.g., Rauma, have fewer passes than potentially available.

Considering the different ECR operations times and the repeat pass geometries served by Sentinel-1, a total amount of 1854 SAR observations would have been accessible to the ECR network. The number of acquired observations is 1561 which corresponds to an overall success rate of 84.2 percent. Table 1 shows detailed numbers for each station. Only very few observations are lost because of incorrect ECR activations or severe weather conditions that rendered the ECR signal unusable. The main reason why some ECRs contribute less data than possible was the programming of activation cycles with respect to the Sentinel-1 operation plan. Until mid May, only Sentinel-1A was operating in standard IW TOPS mode over the Baltic area, while Sentinel-1B was acquiring wide area data for the seasonal sea ice monitoring campaign [4]. Thus, several ECRs had to be reprogrammed during the course of the project to support the additional Sentinel-1B passes, which was not immediately possible due to site access, explaining the lower success rate at sites such as Mårtsbo or Rauma.

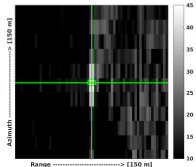
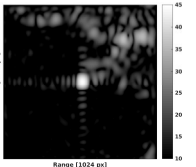
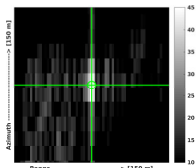
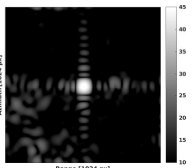
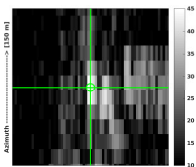
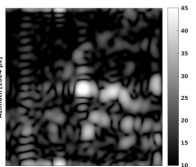
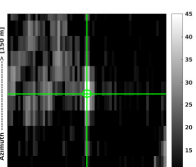
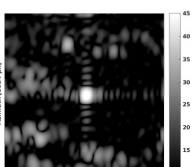
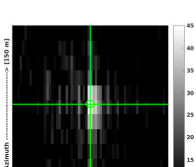
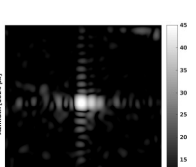
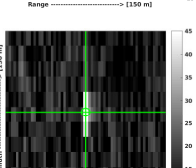
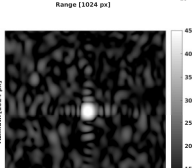
Table 1. Summary on SAR data collected in 2020 within the project’s ECR network. Active periods are the times the ECRs operated successfully. Passes list the number of repeat pass geometries acquired by Sentinel-1 in ascending and descending orientation at a respective site. Sentinel-1 observations refer to the number of SAR images available in the catalogue whereas acquired observations list successful ECR activations with full performance signals in the SAR data. For the station map, refer to Figure 1.

ECR Station	Active mm/dd–mm/dd	Passes [#] (Asc/Desc)	Sent.-1 Obs. [#]	Acquired Obs. [#]	Success Rate [%]
Loksa (LOKS)	02/14–09/12 12/28–12/31	3/2	171	164	95.61
Vergi (VERG)	03/03–08/01 12/28–12/31	3/2	81	81	100.00
Emäsalo (EMAE)	01/23–12/31	3/2	222	185	83.33
Loviisa (LOVI)	02/01–10/20	2/2	132	106	80.30
Rauma (RAUM)	04/21–12/31	2/2	142	76	53.52
Władysławowo (WLAD)	03/20–12/31	2/2	164	142	85.59
Leba (LEBA)	05/15–12/31	2/2	141	116	82.27
Mårtsbo (MART)	01/07–12/31	3/3	322	218	67.70
Kobben (KOB)	06/01–12/31	2/2	160	154	96.25
Vinberget (VINB)	10/01–12/31	2/3	57	57	100.00
Oberpfaffenhofen (DLR2)	01/10–02/25 06/17–09/01	2/1	85	85	100.00
Oberpfaffenhofen (DLR3)	01/10–12/31	2/1	177	177	100.00

Table 2 shows examples for the visibility of the ECRs in the analyzed Sentinel-1 SAR data. All ECR installations provide a clearly visible point response, which confirms good feasibility of the chosen installation sites. In particular, the installations close to coastline, e.g., Loksa, Vergi, or Władysławowo, are very favorable sites, because the surrounding water areas provide very dark backgrounds in SAR, rendering visible the details of the ECR signals. The accurate extraction of SAR timings from the point response requires only the visibility of an undistorted main peak, but the clean shapes and symmetries of the signals give confidence that, in principle, the novel ECR targets are behaving like well-established passive corner reflectors (CR) reference targets. The more challenging locations such as Vinberget (surrounded by forest) or Rauma (industrial harbor area) also pose no problems for measuring the ECRs thanks to the relatively strong signal return of the devices, for which a radar cross section (RCS) of 42.4 dBm² is estimated at the DLR calibration site [5]. The only ECR site that turns out to have limitations is Kobben. Because of concerns regarding radio interference with nearby infrastructure, the installation needed to be shielded by a meshed fence to prevent any signal amplification at low elevation angles. This fencing also causes additional interfering sidelobes in certain pass geometries. Therefore, only some of the observations acquired at Kobben can be used in the SAR positioning. In conclusion, the SAR data analysis preparing the ECR observations is performed very reliably, and only a few ECR observations are marked unusable based on the imaging quality parameters.

The range and azimuth SAR timings of the ECRs as observed by Sentinel-1 are extracted from the signatures in the SAR images by applying point target analysis (PTA). For a detailed description of PTA, refer to [2,5,6]. Corrections for Sentinel-1 systematic effects, tropospheric and ionospheric delays and solid Earth tides are applied to the raw range and azimuth observations using the procedures described in [1].

Table 2. Sentinel-1 SLC image samples showing the ECR point responses for ascending and descending IW TOPS data at some of the selected installation sites. Images display the radar backscatter (σ_0) in units of decibel [7]. Left columns: original Sentinel-1 SLC SAR image samples showing an area of $150\text{ m} \times 150\text{ m}$ around ECR peak marked in green. Right columns: image areas of 32×32 pixels over-sampled by a factor of 32 as generated by point target analysis to extract the ECR peak position. All images are logarithmically scaled for 10 to 45 dB. In each image, the horizontal axis shows the range from 0 to 150 m and the vertical axis the azimuth from 0 to 150 m.

ECR	Ascending Image Sample	Descending Image Sample
Loksa		
Vergi		
Rauma		
Władysławowo		
Kobben		
Vinberget		

Finally, as the ECR is an active instrument, an electronic delay calibration needs to be performed. As accurate delay calibration parameters are not yet available from the ECR manufacturer, they are empirically estimated using ECRs, which are installed at GNSS pre-observed positions. For this purpose, the stations at DLR Oberpfaffenhofen, Mårtsbo, and Vinberget (both Sweden) and Vergi and Loksa (both Estonia) are used, the positions of which are known from GNSS surveys within 5 cm or better depending on instrumentation and observation time. The SAR data products containing the data of 2020 are processed for range and azimuth residuals using the pre-determined coordinates. The residuals of the individual stacks are cleaned from outliers using the median and the 95% confidence interval, assuming normal distribution. Subsequently, mean offset estimates are performed

per stack, which have an estimated precision (95% confidence) of 4 cm in range and 10 cm in azimuth.

The results show significant offsets among the different ECRs and the observed pass geometries, which are attributed to ECR delay characteristics (see Figure 2). Because of these results, linear angular-dependent delay models, discriminating ascending and descending data, are fitted to the averaged residuals by using least-squares adjustment (see Table 3). The model coefficients then allow for a delay compensation in most ECR measurements with an accuracy of approximately 10 cm, but systematic differences of up to 40 cm may remain in certain geometries. The procedure is validated against data acquired for four passive CRs during the same 2020 period, for which no significant offsets or variation across pass geometries are found. These findings for passive CR are in line with published results of Sentinel-1 data quality [8,9]. Therefore, it is concluded that the observed offset effects are not part of the Sentinel-1 system but are introduced by the active ECRs. In order to mitigate the impact in our study, the model coefficients estimated from the selected reference ECRs (Table 3) are applied to the range and azimuth observations of all ECRs installed at the Baltic Sea test network.

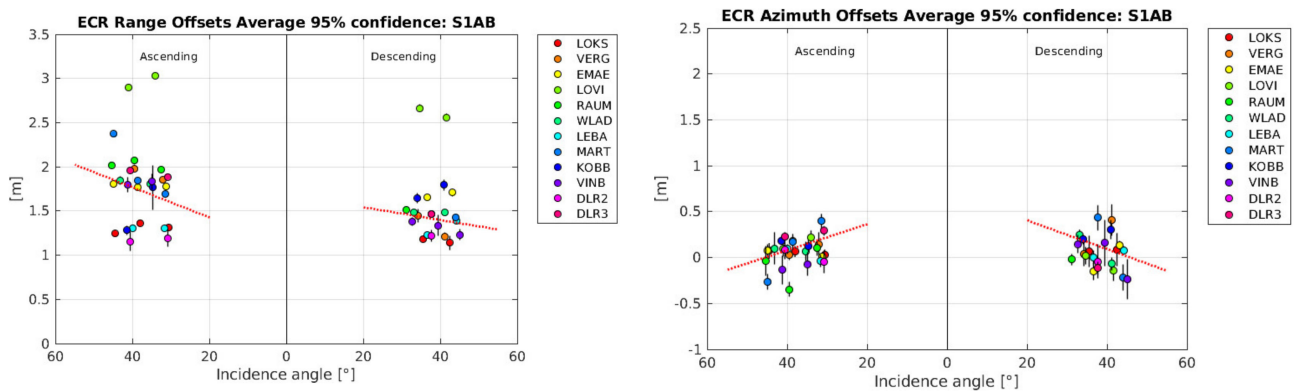


Figure 2. ECR offsets for the different pass geometries observed with the ECR network (colors indicate individual stations). Average offsets estimated with least-squares adjustment from residuals of surveyed ECR positions and measured SAR data filtered for outliers. Range offset estimates per geometry (left) and azimuth offset estimates per geometry (right). Black bars show the 95% confidence intervals of the estimation results. Red lines show the angular-dependent ECR delay models, as listed in Table 3.

Table 3. ECR range and azimuth time delay model coefficients for ascending and descending measurements as derived from ECR residuals of the installation sites DLR2, Mårtsbo, Vinberget, Vergi and Loksa, see Figure 2. The a_0 denotes the mean offset and the a_1 denotes the linear component that depends on the incidence angle of the Sentinel-1 swath, i.e., 20 to 45 degrees.

Configuration	a_0 [s]	a_1 [s/°]
ECR Range Delay Ascending	7.2416×10^{-9}	1.1405×10^{-10}
ECR Range Delay Descending	1.1243×10^{-8}	-4.7810×10^{-11}
ECR Azimuth Delay Ascending	9.5494×10^{-5}	-2.102×10^{-6}
ECR Azimuth Delay Descending	1.0584×10^{-5}	-2.3110×10^{-6}

With all SAR data prepared and an ECR delay calibration established, the SAR range and azimuth timings and the corresponding corrections are analyzed for the overall SAR observation quality of the Baltic ECR network. The following steps are performed in order to assess ECR data quality:

1. The computation of range and azimuth residuals with respect to the surveyed ECR coordinates, applying the corrections for Sentinel-1 systematic effects, tropospheric and ionospheric delays and solid Earth tides. Note that the analysis is performed

with the surveyed ECR origin coordinates corrected for the geometric ECR phase center offsets specified in the ECR manual for ascending and descending passes, following the methods proposed in [10]. The ECR origin coordinates are observed during installation with differential GNSS and are considered to be accurate within 5 cm or better depending on the instrumentation and observation time.

2. The removal of outliers from the residuals of each individual geometry using the median and a 95% confidence interval, assuming normal distribution.
3. The estimation of average ECR offsets from the cleaned residuals of each geometry along with the 95% confidence interval using least-squares methods.
4. The computation of the range and azimuth standard deviation for each set of residuals to empirically quantify the single observation precision (1 sigma) of each geometry.

The estimated average offsets are visualized in Figure 2 and show mainly electronic delays of the ECRs, with additional bias contributions stemming from the orbit, the finite correction accuracy, and the surveyed coordinates. The sum of additional biases is assumed with a maximum of 8 cm. The standard deviations for the residuals of each geometry are shown in Figure 3.

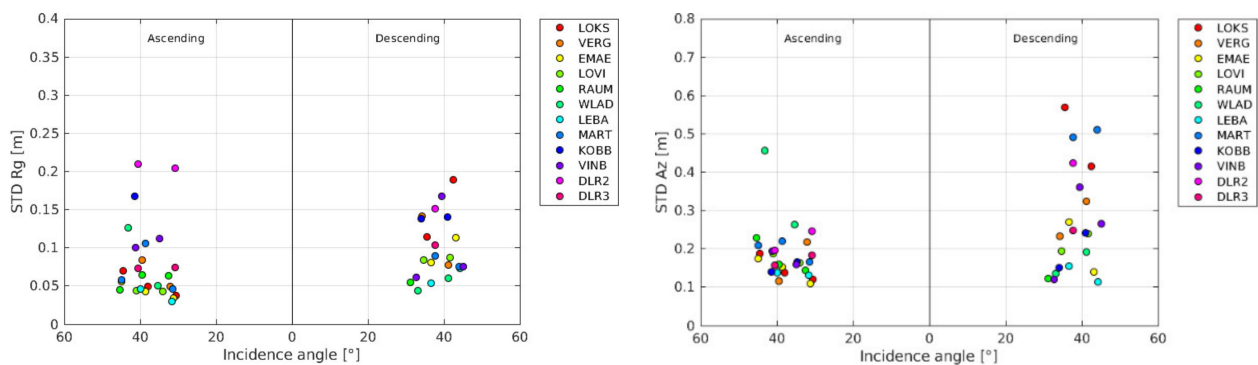


Figure 3. Empirical estimation of ECR SAR observation quality for the different pass geometries observed with the ECR network (colors indicate individual stations) after applying all data corrections. Standard deviation of residuals derived from surveyed ECR positions and measured SAR data filtered for outliers. Standard deviation of range measurements per geometry (**left**) and standard deviations of azimuth measurements per geometry (**right**).

Several conclusions can be drawn from these results. The SAR range observations of the ECRs generally have a high precision when considering only the individual geometries. For most of the data stacks, the average range offsets are estimated with a precision of better than 4 cm (95% confidence), which also confirms that most of the detected differences among ECRs and geometries are significant. Only a few ECRs can provide relatively homogeneous range data across all incidence angles, e.g., Emäsalo or Loksa, and there is low consistency among the different ECR delay patterns (see Figure 2).

Despite being built to same specification and stemming from one manufacturing series, the ECR delays can vary between 1.2 (Loksa, DLR2) and 3 m (Loviisa). The lower precision of the Kobben results is possibly caused by interference of the fencing, which particularly affects the 34° ascending geometry. The lower precision of the DLR2 is due to the repaired electronics, which changed the electronic characteristics of this device. Similar findings on range delay variations of 1.2 and 2.1 m for this type of ECR are also reported in [10]. Our experimentally determined delay model can therefore remove the delay effects only within ± 0.5 m in absolute accuracy and not all ECR match the average behavior of the linear model. Moreover, absolute SAR positioning accuracy will be limited to decimeters if these systematic effects are not compensated for. Stations such as DLR2, Loksa, or Loviisa will perform worse because of their more distinctive delay patterns.

The azimuth observations of ECRs are much more consistent and seem less affected by the ECR electronic characteristics (Figure 2). The remaining azimuth offsets are comparable

to the earlier results obtained with passive CR [5]. The precision of azimuth bias estimation is limited to 15 cm (95% confidence) mainly because of the 20 m azimuth image resolution. Considering this limited precision, the experimentally determined ECR model can remove most of the systematic effects, and an azimuth observation accuracy in the order of 20 cm is attainable.

The precision (1 sigma) of a single ECR measurement in range generally varies between 5 to 10 cm standard deviation, as shown in Figure 3 left. Again, the interfering fence at Kobben and the impact of the repaired electronics of DLR2 are visible in the results. The ECR measurements in azimuth show a typical standard deviation of 10 to 30 cm (see Figure 3 right), but there is a difference between ascending and descending data for several ECRs. Such a difference is also visible in the range results. The reason for this behavior is unclear, but it is likely related to the ECR themselves because such results have not been reported so far with Sentinel-1 and passive reflectors [5,8,9].

In summary, the attainable precision of Sentinel-1 SAR observations of ECR is largely equivalent to observations of passive CR but absolute accuracy is limited by the delay effects introduced by the active ECR electronics. The effects vary between the individual instruments, which makes a satisfactory ensemble characterization impossible. In order to achieve better absolute accuracy and improve feasibility for SAR positioning, the ECR should be electronically characterized and calibrated by the manufacturer. Nevertheless, a reliable operation was achieved with most of the devices which yielded a considerable amount of ECR measurements with Sentinel-1 that allow for the processing of absolute 3D positions.

2.2. SAR Positioning

In this chapter, the results of the SAR positioning of 12 ECR stations located in the Baltic sea region and at DLR in Oberpfaffenhofen are summarized. The positions were computed using the refined absolute positioning of the SAR processor described in [1]. The SAR observations are corrected for atmospheric, geodynamic, Sentinel-1 specific, and systematic effects of the SAR-transponders, such as phase center offset and electronic delay (see Section 2.1). Depending on the station, the number of data takes (DTs) varies due to different periods of operations and different latitudes and, therefore, different numbers of available incidence angles for the ECR transponders (see Table 1).

For each ECR, all available data since the start of operation until the end of 2020 are used. For all 12 stations, average coordinates for the year 2020 and precision values are estimated by a least squares procedure in the ITRF2014 system. The precision (internal accuracy) varies between a few millimeters and one centimeter per coordinate axis. The precision is fairly stable, even though the number of data takes vary over the stations. This independency is due to the fact that the estimator becomes already stable when more than 20 DTs per station are used. Table 4 shows the coordinates converted to the target ellipsoidal coordinates referring to the GRS-80 ellipsoid.

A more detailed view about the estimated precision of the ECR station coordinates is provided by the confidence ellipsoids shown in a local north-east-up coordinate frame. Figure 4 shows the results for a confidence level of 95% for all stations. The confidence ellipsoids only spread over a couple of millimeters or few centimeters. The varying eccentricity of the ellipsoids is related to the ratio of observations taken in ascending and descending geometry. The more balanced the number of observations per geometry, the more circular the confidence ellipsoid will become.

Table 4. Estimated average GRS-80 ellipsoidal coordinates for year 2020 (longitude, latitude, height) for all stations using all available observations in the year 2020. The epoch is defined as the mid of the total observation period (see Table 1). The number of all valid observations is defined as the number of acquired observations (as shown in Table 1) minus outliers (A: Azimuth, R: Range observations).

ECR Station	Latitude [°]	Longitude [°]	Height [m]	Valid DTs [#] A/R	Epoch
Loksa	59.582555692	25.705865677	20.0761	160/163	2020.475
Vergi	59.601493430	26.100800251	28.9661	66/77	2020.422
Emäsalo	60.203674412	25.625661421	34.2932	181/165	2020.586
Loviisa	60.440749584	26.284251613	46.8399	101/99	2020.508
Rauma	61.133538554	21.425982308	24.0824	75/72	2020.656
Władysławowo	54.796783467	18.418754840	34.6395	133/139	2020.639
Łeba	54.753658763	17.534876057	34.3894	116/109	2020.681
Mårtsbo	60.595133036	17.258527904	75.4769	206/194	2020.581
Kobben	60.409897086	18.230323460	25.6586	81/78	2020.586
Vinberget	62.373892667	17.427849782	149.6544	54/54	2020.852
DLR2	48.084935323	11.281195447	626.6280	83/71	2020.542
DLR3	48.087916451	11.279137080	623.8140	174/172	2020.517

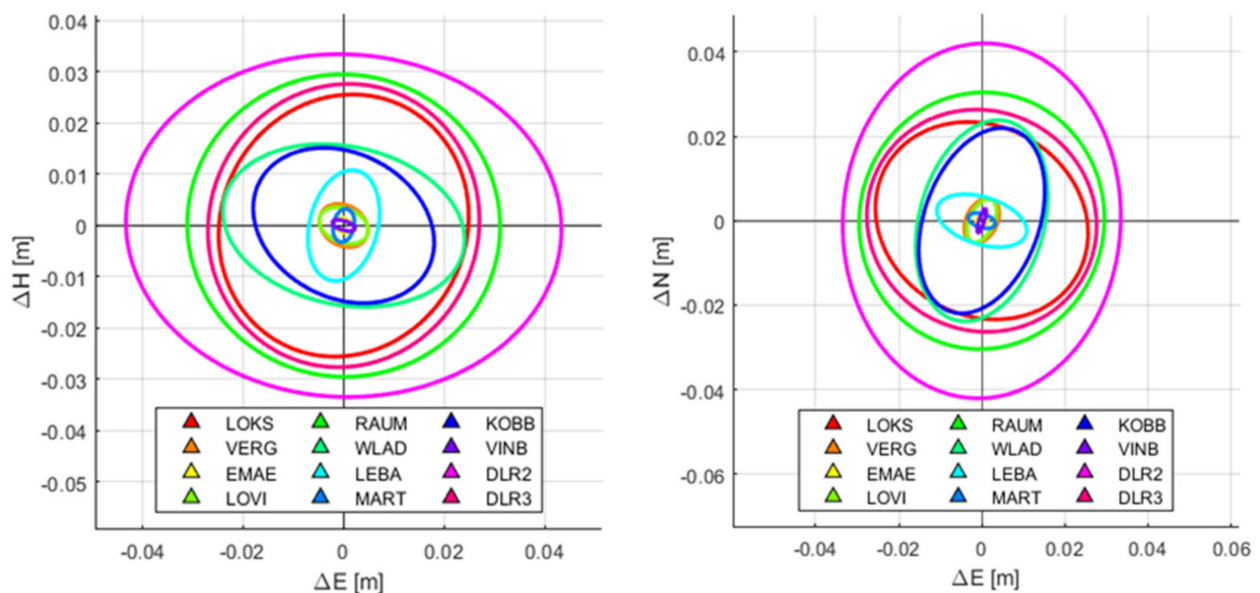


Figure 4. Confidence ellipsoids (95% confidence level) for all 12 stations using all available observations in the year 2020. The confidence is shown in the local and east/height (**left image**) and north/east (**right image**), coordinate frame with respect to the estimated coordinates.

The confidence ellipsoids can also be presented with respect to the difference to the reference coordinates—surveyed with GNSS, as shown in Figure 5. Here, one can identify that the absolute positioning accuracy can vary on a larger scale than the estimated precisions. The absolute accuracy in height varies between centimeter offsets and a few decimeters. Large offsets in height such as in Loviisa and Łeba deviate from the other stations. On the other hand, these stations also differ from other stations by having high absolute accuracies, looking at the horizontal offsets.

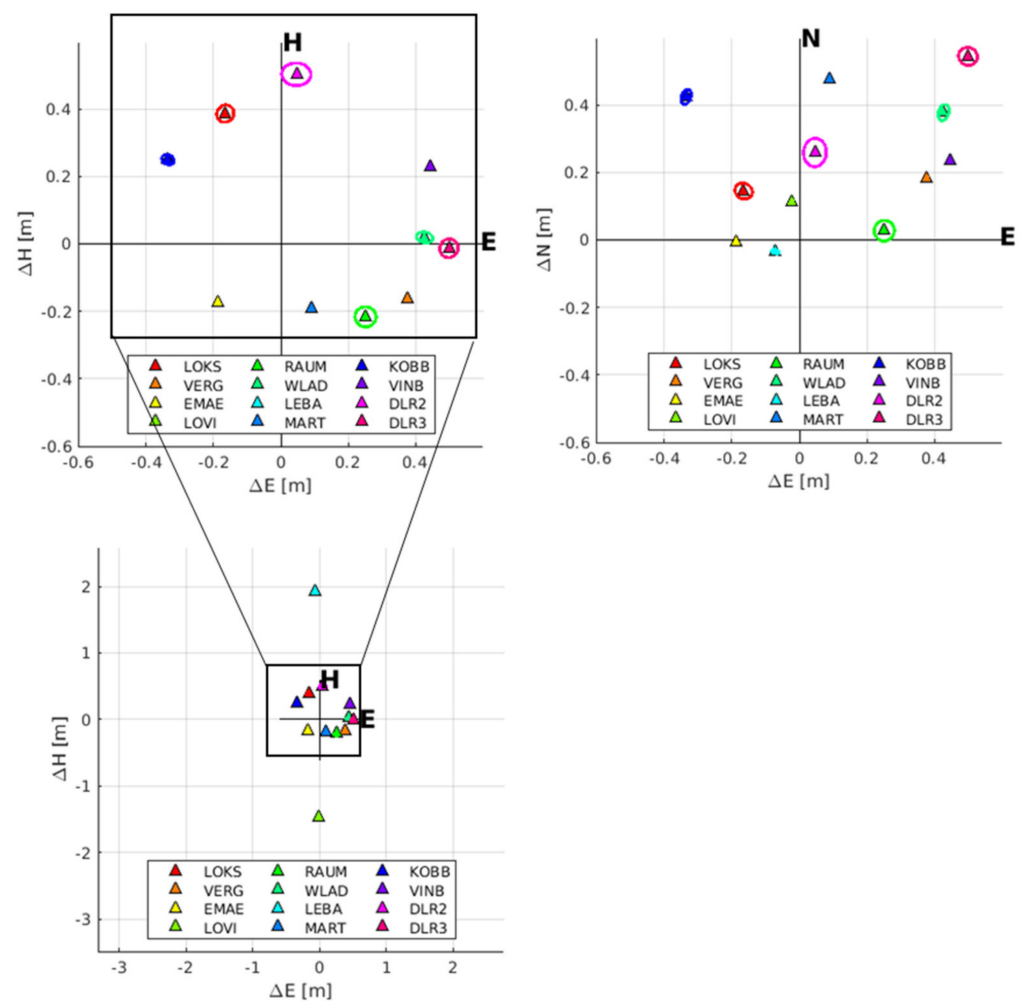


Figure 5. Confidence ellipsoids in local east/height (**top left**), zoomed out local east/height (**bottom left**), and local north/east (**right**) coordinates of all ECR stations using all available observations from 2020. The center position of the ellipsoids is given with respect to reference coordinates, previously measured by GNSS campaigns and therefore represent offsets with respect to reference coordinates.

Figure 6 shows the residuals of valid data takes for a few selected stations with long observation time periods with respect to the observation period. The residuals are expressed in meters by multiplying the observations residuals with the speed of light for range observations or the speed of the satellite for azimuth observations. The residuals are computed after the refined absolute positioning is finished. This means that flagged dates, gross outliers (larger residuals than half a pixel of sentinel 1 SAR-image), and outliers (3σ -median criterion) have been removed. Furthermore, a bias correction due to the systematic behavior of residuals per incidence angle was applied. Emäsalo (Figure 6, top row) is one of the longest working stations and performs stably with good internal accuracies. Władysławowo (Figure 6, mid row) performs nominally and shows stable residuals and internal accuracies of a few centimeters. The ECR at Mårtsbo (Figure 6, bottom row) belongs to the longest observing stations. It shows the smallest residuals in range and, interestingly, the largest residuals in azimuth compared to other stations.

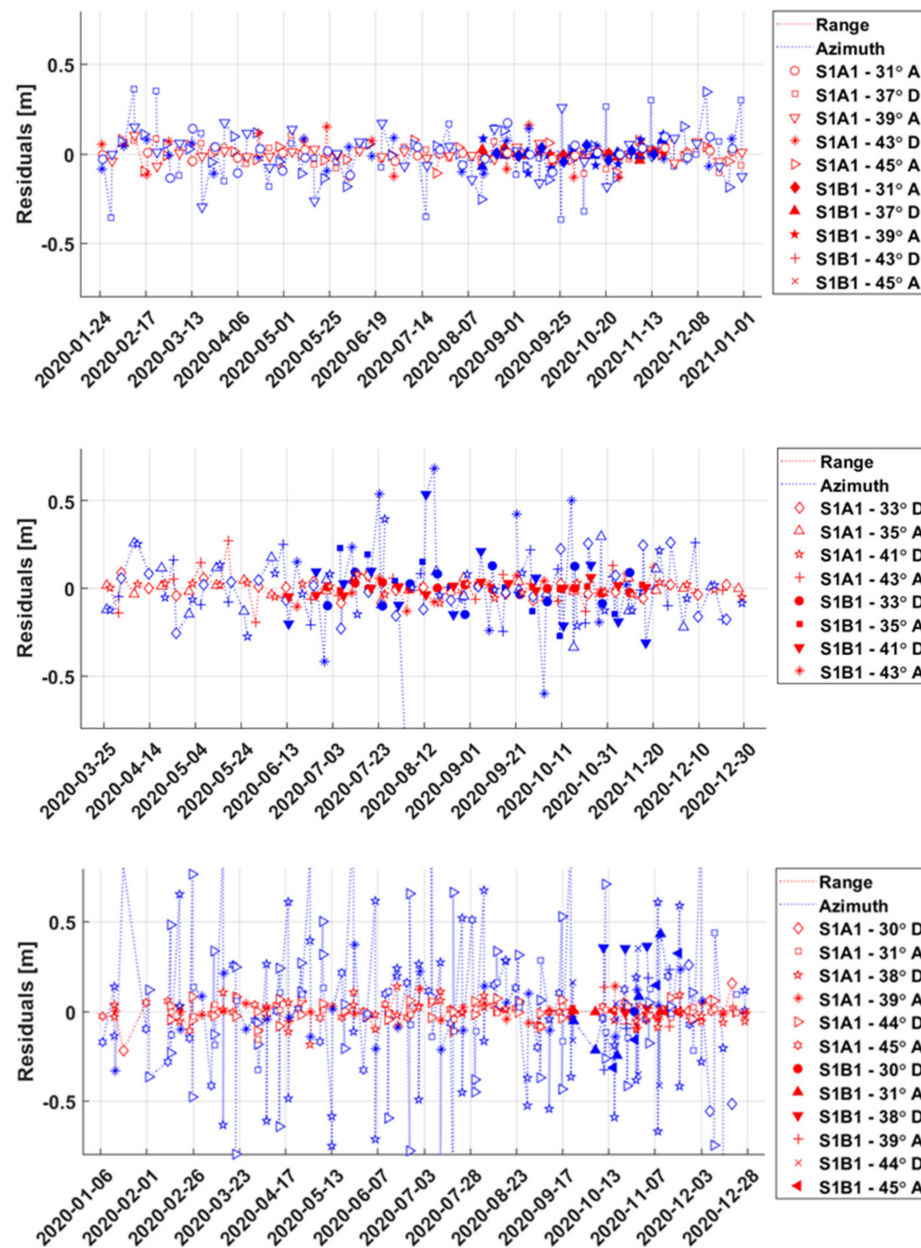


Figure 6. Observation residuals at selected stations. Range observations are colored in red; the different symbols indicate different incidence angles. Azimuth observations are shown in blue; symbols indicate the same incidence angles as for the range observations. Top row: Emäsalo, Finland; Mid row: Władysławowo, Poland; Bottom row: Mårtsbo, Sweden.

In order to answer the question of whether temporal changes can be observed with ECRs, coordinate solutions for monthly (1 M), bimonthly (2 M), trimonthly (3 M), and four-monthly (4 M) data subsets are computed. The goal is to identify what is the minimum number of observations to reach a stable positioning solution, and second aim is to investigate how stable the solutions are over time and if there is a chance to observe vertical land motion. From the average coordinate solutions, it was identified that the SAR positioning stabilizes when more than 20 DTs (azimuth + range) are available. Figure 7 illustrates the behavior of the standard deviations with respect to the number of DTs for the different temporal resolutions at all stations. Generally, the coordinate standard deviations improve with increasing number of DTs, but one can define a limit where there is only marginal improvement achievable. From the results, it is fair to assume that this limit is reached with about 80 data takes.

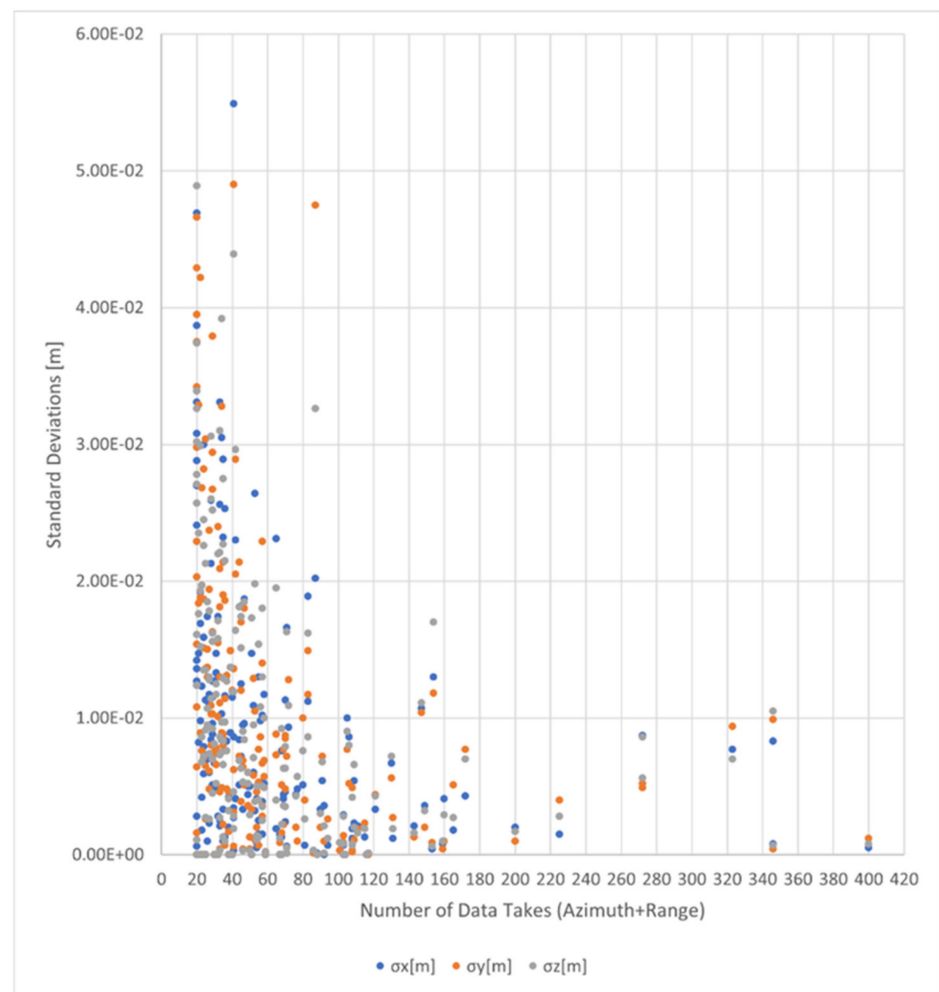


Figure 7. Standard Deviations of absolute positioning of all ECRs and all temporal resolutions (1 M, 2 M, 3 M, 4 M, yearly) per number of data takes (sum of range and azimuth observations).

In Figure 8, as an example, the positioning performance for the well observed station Emäsalo is shown for different temporal resolutions (1 M, 2 M, 3 M, and 4 M). The positioning offsets with respect to the GNSS-based reference coordinate are presented for different epochs in the local north, east, and up frame. Once-monthly solutions tend to have larger standard deviations than their respective 2 M, 3 M, or 4 M solutions at the same station. Three- and four-monthly solutions, consisting of around 80 DTs or more, perform, for most stations, as well as the solutions using all available observations of the year 2020. For every SAR positioning solution, a linear correction was applied based on the trend of the nearest IGS station to shift the reference coordinates to the respective epochs of the SAR positioning. Therefore, the 1 M and 2 M solutions ideally should show a constant offset to their reference coordinates over time, if one assumes that the IGS station coordinate trends are applicable to the ECR stations as well. Any residual trend for the coordinate axes could imply that the IGS linear correction model does not reflect the reality good enough or that the uncertainty of the estimated ECR positions is too high to observe such trends. To evaluate this, the root mean square (RMS) value for the 1 M and 2 M solution offsets was estimated. As can be seen in Figure 8 (two top panels), for Emäsalo, the RMS in all three directions (north, east, up) is between 11 and 17 cm, which is significantly above the IGS trend model at a level of 1–2 cm per year per coordinate axis. Similar results are obtained for all other stations (not shown here).

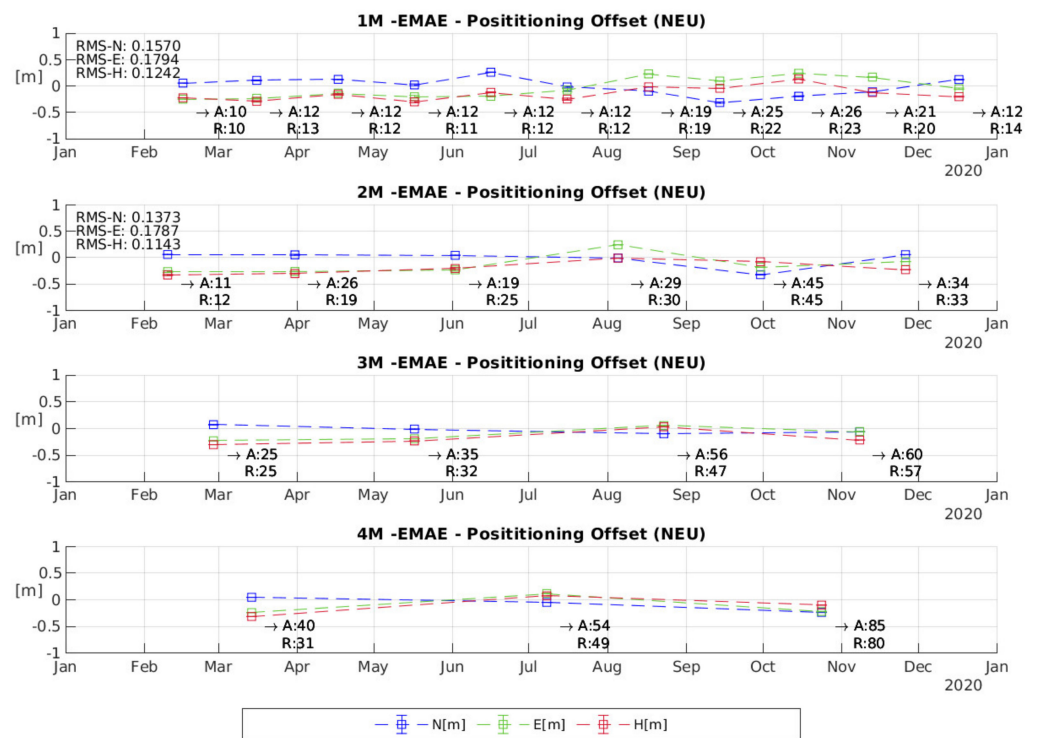


Figure 8. Positioning offset of the ECR located in Emäsalo for the different temporal resolutions derived from SAR data: monthly (1 M), bimonthly (2 M), trimonthly (3 M), and every four months (4 M) in the year 2020. The offsets are displayed in local North (blue), East (green), and Height (red) with respect to given reference coordinates from GNSS campaigns at the mean date of each observation period. For 1 M and 2 M, the Root Mean Square (RMS) values in meters are displayed in the top left corner of the respective graph. “A”: and “R”: beneath each solution indicate the number of radar measurements used in azimuth and range for the particular solution.

Monthly is the shortest time interval of observations in order to reach realistic positioning results. Most ECR stations only gather 10 valid range and 10 valid azimuth observations over a period of one month, which is a minimum for stable performance of the positioning processor. The higher the latitude, more observations within a month are possible. This needs to be considered for possible applications of the SAR positioning technique. Table 5 shows RMS values of the positioning results for all stations and their 1 M and 2 M positioning solutions. DLR2 is excluded because its delay characteristics changed significantly after repair. One can see in the height component that the RMS behaves differently for every station and varies between 3.5 and 17.4 cm for the 1 M solutions with a mean of 11 cm. For the 2 M solution, the RMS improves in the mean to 9 cm. This shows that, with an increased number of observations, the positioning becomes more stable for most stations. A longer observation period of a few years would allow a comparison with 3 M and 4 M solutions and might be helpful for further analysis. However, after all, monthly and bimonthly solutions still vary on a decimeter level with respect to each other.

There are observation periods for which the processor does not converge for a position result even with sufficient number of data takes. Therefore, the positioning is terminated providing unreliable results. The bias correction (refer to [1]) in general helps to reach convergence for the position solution. For a few stations (LOVI and KOBB) and some specific observation intervals, the bias correction even deteriorates the achieved solution. Therefore, for these two stations, solutions without bias correction are computed (see Table 5).

Table 5. Root mean square (RMS) values of the once-monthly (1 M) and bimonthly (2 M) solutions of each station. Loviisa and Kobben were computed without bias correction due to computational issues for single observation intervals. DLR2 is excluded in the table, as its performance significantly changed after each repair of the transponder.

ECR Station	1 M RMS			2 M RMS		
	dN [m]	dE [m]	dH [m]	dN [m]	dE [m]	dH [m]
Loksa	0.1617	0.2267	0.1724	0.0605	0.1702	0.1832
Vergi	0.1544	0.0817	0.0911	0.0667	0.1032	0.0920
Emäsalo	0.1570	0.1794	0.1242	0.1373	0.1787	0.1143
Loviisa	0.1689	0.0647	0.1139	0.0999	0.1328	0.0620
Rauma	0.0797	0.0580	0.0359	0.0904	0.0394	0.0497
Władysławowo	0.2069	0.1272	0.1309	0.1482	0.2070	0.0725
Łeba	0.1300	0.1285	0.1201	0.0806	0.0883	0.0280
Mårtsbo	0.1470	0.0995	0.0889	0.2389	0.0292	0.0736
Kobben	0.1011	0.2485	0.1748	0.0840	0.2172	0.1269
Vinberget	0.0220	0.0549	0.0407	-	-	-
DLR3	0.1348	0.3525	0.1275	0.0645	0.3165	0.1176
Mean:	0.1330	0.1474	0.1109	0.1071	0.1483	0.0920
Min:	0.0220	0.0549	0.0359	0.0605	0.0292	0.0280
Max:	0.2069	0.3525	0.1748	0.2389	0.3165	0.1832
Median:	0.1470	0.1272	0.1201	0.0872	0.1515	0.0828

No Bias Correction applied for Loviisa and Kobben

From the positioning results of all ECR stations by processing all available SAR observations from the year 2020 (see Table 5), several conclusions can be drawn, which need to be considered for any future data analyses of this kind.

First of all, the ECRs seem to perform unequally, meaning that, for example, electronic delays might differ significantly for different ECRs. For the SAR positioning in this project, it was assumed that the delay is determined from the average coordinate differences of just a few selected reference stations and then applied to all ECRs during processing (see Section 2.1). Positioning results show that there is uncertainty about a common electronic behavior of the ECRs, and therefore, each ECR shall be calibrated at a reference station before it is installed at a designated observation point. Only if ECRs are verified to perform similarly in this respect can a representative electronic delay be computed from a few ECRs at reference stations. Varying electronic delays per ECR strongly influence the absolute coordinate accuracy rather than the internal precision estimate of the positioning result.

When looking at systematic effects, one always has to keep in mind to take care of the different viewing geometries due to different incidence angles. To use both ascending and descending orbit observations, the phase center correction has to be applied, as the phase center differs by several decimeters in the positioning, depending on the incidence angle.

Currently, outlier detection is split in two steps, i.e., gross outliers (half pixel resolution of Sentinel-1) and outliers (3-sigma criteria per incidence angle) are treated separately. Additionally, observations are flagged, where precise orbit information seems to be insufficient accurate. Optionally, single data points can also be flagged manually, if required. Outlier detection is critical to the positioning performance and needs to be performed very carefully.

As a promising result of this study, it can be stated that the positioning exhibits high internal accuracies. The internal accuracies for the solutions using all stations vary between a few centimeters down to millimeters in the local north, east, and height reference frames. This implies that having a continuous observation period with good data coverage, relative coordinate variations can be observed on bi-monthly (monthly, under optimal conditions) time intervals with a few centimeters' precision. For absolute positions, a well-calibrated and long-term stable instrument is needed, which is not the case for the ECRs used during the study.

2.3. GNSS Positioning

Twelve GNSS stations near ECRs and/or tide-gauge stations are available for the Baltic Sea test network. Because the coordinates of these GNSS stations are treated as reference values for the SAR positioning technique, they need to be determined with the highest possible accuracy. For this purpose, a regional GNSS network is defined such that a good and stable geometry for determining the coordinates is enabled. Reference stations with a long and stable time series of coordinates including well-defined velocity vectors are chosen. For this purpose, Northern European permanent IGS and EPN network stations are inspected for data quality, data gaps and missing sessions as well as for the geometry of the created network, the mutual distances between the stations and the availability and quality of station velocity vectors. Additionally, selected national stations of the EUPOS system (FinnRef, ESTREF, ASG-EUPOS, SWEPOS) are included where appropriate. Finally, with this procedure, 45 stations are qualified for the regional network to be used for this study (Figure 9).

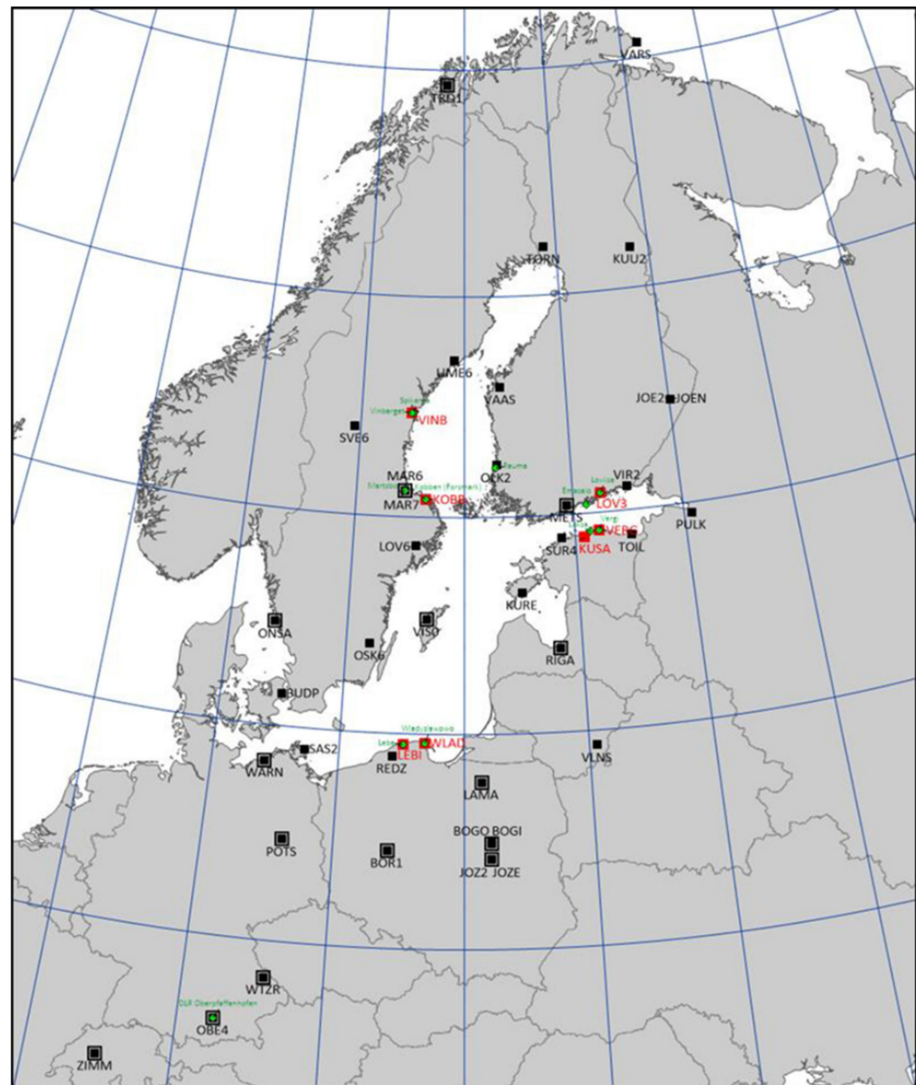


Figure 9. Map with distribution of all included GNSS stations. Large black squares are the IGS network stations, smaller black squares are the EPN stations, and red squares are the stations belonging to the EUPOS (FinnRef, ESTREF, SWEPOS and ASG-EUPOS). Only LEBI station belongs to Leica commercial network. Little green diamonds indicate the locations of the ECR transponders.

The processing of observations was performed as a daily network solution with the Bernese GNSS Software version 5.2 [11] in the double-difference mode (DD method). As a reference frame, ITRF2014 [12] was used, in which all IGS global products are available for the calculations: precise orbits, the Earth's rotation parameters, and the corrections of GNSS satellite clocks. IERS2010 conventions [13] are applied as background models.

The daily network solutions are related to the mid of the development period of each daily session. Based on these solutions, the time series of Cartesian coordinates covering the entire year of 2020 were generated. From these time series, time series geodetic coordinates (latitude, longitude, and ellipsoidal height) were computed, related to the GRS-80 reference ellipsoid. As an example, the geodetic coordinate time series for a northern (Mårtsbo—MART) and a southern (Władysławowo—WLAD) GNSS station of the Baltic Sea test network, which are co-located to an ECR, are shown in Figure 10.

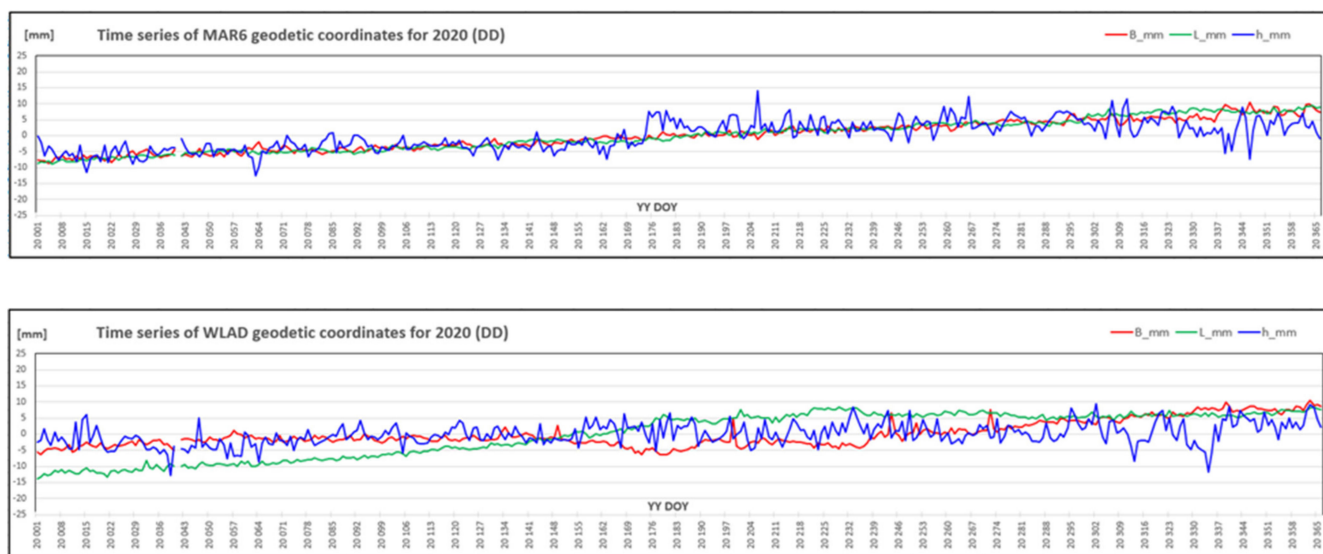


Figure 10. Residual daily coordinate time series with respect to reference coordinates for the year 2020 for Mårtsbo (MAR6, top panel) and Władysławowo (WLAD, bottom panel) permanent GNSS stations. Ellipsoidal latitude is shown in red, longitude in green, and height in blue color. Vertical axis shows coordinate residuals in the range ± 25 mm, horizontal axis specifies the day of year 2020 from day 001 to day 365.

The graphs in Figure 10 clearly show horizontal displacements of stations caused by the movement of continental tectonic plates and trends in vertical movements at stations located in the Gulf of Bothnia. Due to the fact that the period of data processing is too short (covering only one full year), it is not possible to accurately determine the values of linear trends, and periodic terms (annual, semi-annual) from the prepared time series of station coordinates. Therefore, for the purpose of average coordinate solutions, values from the ITRF2014 kinematic model [12] are used, which sufficiently describe the dominant movements in the studied region'.

The final average coordinate solutions for the reference epoch 2020.5 based on the double difference approach are summarized in Table 6. For the purpose of comparing the results calculated by the DD method and for the verification and interpretation of the effects in the height component observed at several GNSS stations, the precise point positioning (PPP) method is applied as well. This method is slightly less accurate than the DD method, but at the same time, it is free from the influence of the selection of the reference station network on the coordinates of the determined stations. The results show that, for all stations, for the height component, an agreement between 1 and 3 mm is achievable, from which it can be concluded that all GNSS coordinates are well within the error budget of a centimeter or better.

Table 6. GNSS stations geodetic coordinates (latitude, longitude, and height) in ITRF2014 epoch 2020.50 (from period 1 January 2020 to 31 December 2020) referred to GRS-80 ellipsoid. Solution from DD method. Only GNSS stations coordinates immediately co-located to an ECR stations are shown.

GNSS Station	Latitude [°]	Longitude [°]	Height [m]
Leba (LEBI)	54.753775669	17.534799064	37.8856
Loviisa (LOV3)	60.440771458	26.283844394	49.8794
Mårtsbo (MAR6)	60.595145817	17.258531528	75.5578
Vergi (VERG)	59.601489744	26.100798661	30.0692
Vinberget (VINB)	62.373816278	17.427743125	150.2055
Władysławowo (WLAD)	54.796761422	18.418757500	34.7580

2.4. Tide Gauge Data Analysis

The ECRs are mounted at seven tide gauge (TG) stations in Estonia, Finland, Poland, and Sweden (Loksa, Emäsalo, Rauma, Leba, Władysławowo, Kobben, and Vinberget). All the participating TGs detect sea level automatically. These TGs are connected to the national height networks via leveling to adequately monitor and predict sea level fluctuations and oceanographic processes, as well as vertical land motions (VLM) along the entire shore of respective countries. All the participating countries use the European Vertical Reference System (EVRS), which is referred to the Normaal Amsterdams Peil (NAP). The time epoch for the vertical datum is 2000.0.

Besides observations for the year 2020, relevant TG station documentation and meta-data are also made available by the national TG authorities for each participating TG. These include information about the definition of the TG station location, used sensor types, datums, benchmarks, leveling, maintenance, malfunctioning, etc. It is also essential to identify whether the submitted TG data is “raw” or corrected for certain phenomena (e.g., ocean and Earth tides and inverse barometric correction). All available TG data are un-normalized, i.e., the data represent the actual hourly sea level heights at the TG stations. As the TG data represent relative sea level, the VLM estimates (reaching up to 9 mm/year) can be accounted for separately, e.g., following methodology in [14].

The TG time series are quality-checked and statistically analyzed to filter out data blunders. Several tests are conducted to identify gross errors and systematic biases. Gross errors are removed by analyzing TG readings visually or using numerical constraints. Occasional data jumps, defined as a single reading differing from its adjacent readings (due to vessels maneuvering close to a TG station) by some threshold, are identified and eliminated. Abrupt sea level changes (e.g., >10 cm over an hour) can indicate gross errors; such occasions are examined individually and verified with contemporary weather conditions. For instance, on 17–18 September 2020, the sea level in Loksa rose quite rapidly more than one meter and dropped back to where it started within 8 to 10 h. It was confirmed that extreme meteorological conditions generated the sudden sea level rise. Figure 11 shows hourly sea level variations for a few selected TG stations (including the Loksa event).

The detected gross errors are eliminated from further analysis. Thus, coherent time series for 2020 are obtained for all the participating TGs. Data gaps (e.g., due to malfunctioning of instruments) in the TG data series also occurred, which are identified (see Table 7). The readings’ standard deviation (STD) reflects the inner consistency (for the entire period, or seasonally) of the time series at each TG station (see Table 7). Typically, the STD of the annual sea level series remained around two decimeters, whereas a larger STD is associated with rougher marine conditions at an individual TG station. On the other hand, significantly smaller STD can reveal a sea sheltered location (e.g., Leba).

The TG data series are then used for computing the annual average sea level estimates for each TG station, referring to the national realizations of the EVRS vertical datum at time epoch 2000. Table 7 summarizes the average sea level height (in EVRS datum) for the period 1 January 2020 to 31 December 2020, as well as the leveled heights of the co-located ECRs relative to the TG zero marker.

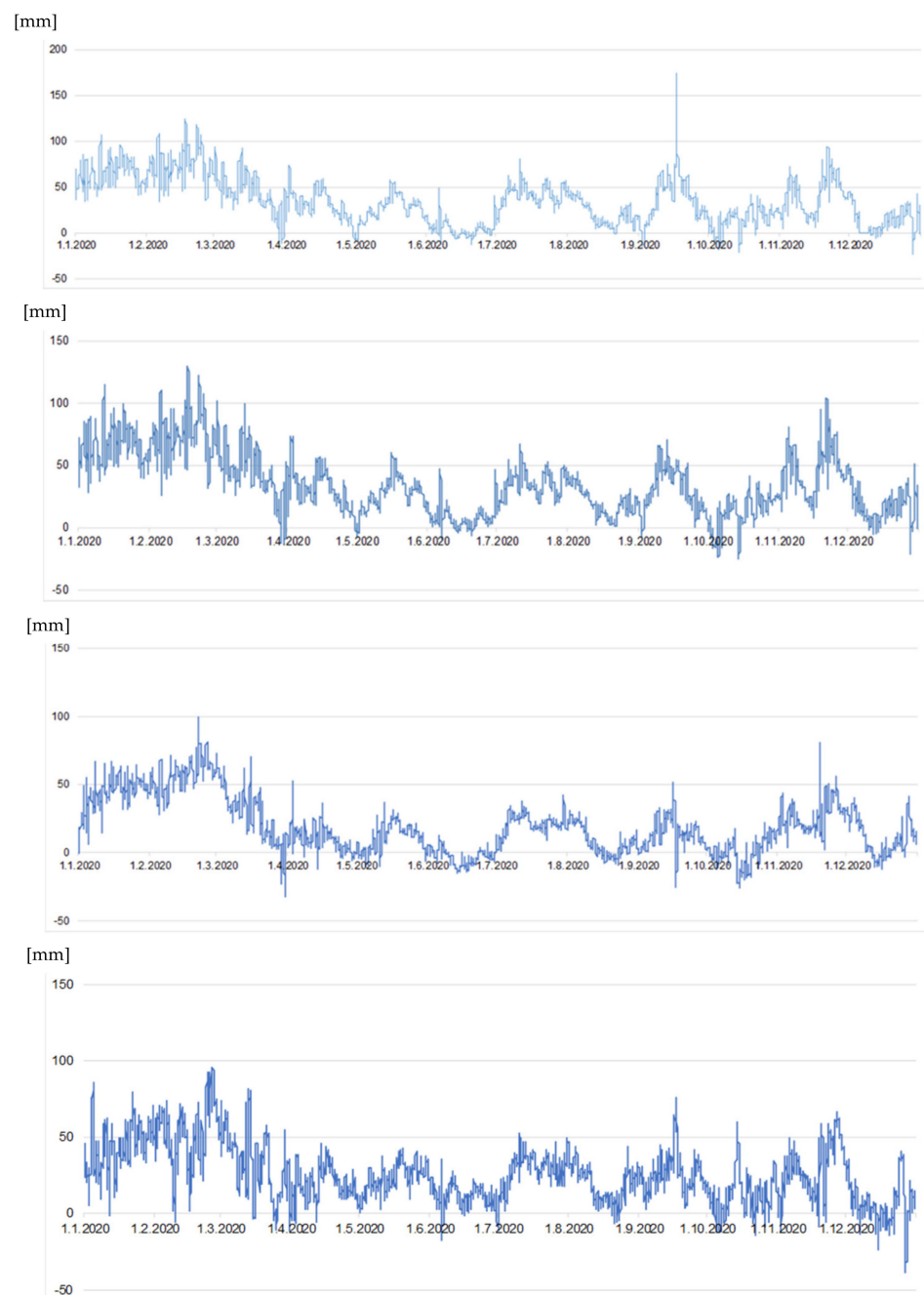


Figure 11. Hourly TG sea level time series (in millimeters) for Loksa, Estonia (**1st row**), Emäsalo, Finland (**2nd row**), Kobben, Sweden (**3rd row**), and Władysławowo, Poland (**4th row**) for the year 2020.

The Gulf of Finland TG stations (Loksa and Emäsalo) at the opposite shores show good agreement; the average sea level is about +34 cm. On the other hand, during the time period in question, an upward spatial sea level gradient from west to east is identified in the Gulf of Bothnia TG stations. The sea level at the Finnish shore appears to be about 7–8 cm higher than the sea level at the Swedish TG stations. The adjacent Finnish TG stations Pori and Turku confirm the Rauma average sea level of +26 cm. Intuitively, such a west–east directional upward tilt (also higher than average sea level in the Gulf of Finland) can thus be due to prevailing (stronger and more frequent) westerly winds during the season in question. The 3 cm mean sea level difference (+22 versus +25 cm) for the adjacent Polish stations could have some local coastal circulation-related reason.

Table 7. Summary of the TG and ECR levelling results for year 2020, referred to the national realizations of the EVRS vertical datum.

TG Station	ECR Reference Height [m]	TG Average Sea Level Height [m]	STD TG Time Series [m]	Missing Data [%]
Loksa	2.6385	+0.343	0.245	1.2
Emäsalo	17.8155	+0.338	0.238	0.6
Rauma	5.0075	+0.258	0.216	1.1
Kobben	2.9606	+0.188	0.200	0
Vinberget	123.5233	+0.175	0.215	0
Władysławowo	5.6382	+0.253	0.186	0.2
Łeba	3.0491	+0.224	0.173	0.3

2.5. GOCE Based Geoid Determination

For observing the absolute sea level and enabling the unification of height systems, the physical heights of the TG stations referring to a common equipotential surface are needed. This equipotential surface is achieved by computing a regional (quasi-)geoid for the Baltic Sea test area, which combines a GOCE-based Earth gravity model (EGM) with local/regional gravity data (land, airborne and/or marine) and a digital elevation model (DEM). In order to check the impact of the geoid determination methods on the resulting equipotential surface, two approaches are applied. In particular, these are the three-dimensional least squares collocation (3D LSC method) [15–17] using the remove–compute–restore method with residual terrain modeling (RTM) of the topographic corrections [18] and the least squares modification of Stokes’ formula with additive corrections (LSMSA method, also called KTH approach), where the remove–compute–restore scenario is used for gridding of the surface gravity anomalies; see, e.g., [19–21]. The evaluation of gravimetric quasi-geoid models is made over two test areas. The north area covers basically the central and northern parts of the Baltic Sea, while the large area extends to include the Polish TGs to the south.

First, local/regional gravity data for the test areas are compiled. This includes the NKG2015 land gravity data owned by Sweden, Finland, Estonia, and Poland (plus the NKG 1999 airborne campaign and a few open marine gravity datasets) [22,23] and the new FAMOS marine gravity datasets available from Sweden, Finland, and Estonia. The gravity observations cover the TGs and ECRs of the Baltic Sea test network with an overlap of more than 110 km in all directions. In areas without real gravity observations, pseudo-observations generated from the EIGEN-6C4 global model [24] with $5' \times 5'$ resolution are added in order to cover a gravity (grid) area overlapping the large quasi-geoid test area with ± 2 degrees in latitude and ± 6 degrees in longitude. The final gravity dataset for the Baltic Sea test area is illustrated in Figure 12. The NKG2015 and FAMOS gravity data are in the national gravity systems. For the most accurate gravity data on land, a transformation is made to the zero permanent tide system and the postglacial land uplift epoch 2000.0. However, these corrections are small and hardly significant for geoid determination. All surface (free air) gravity anomalies are computed using the GRS-80 normal gravity field [25].

In order to compute topographic corrections, the NKG2015 DEM (called NKG_DEM2014) was used over Sweden, Finland and Estonia. In Poland and areas with pseudo-observations, a DEM based on GTOPO and SRTM3 (below 60 degrees latitude) is utilized. The latter DEM was used as the starting point to create NKG_DEM2014. The high accuracy national DEMs from the Nordic and Baltic countries were then overlaid on top of this model to create NKG_DEM2014 [22]. Two different GOCE-based satellite-only GGMs, namely DIR_R6 [26] and GOCO06S [27], both with maximum degree 300, are used in the computations as reference model. As mentioned above, two different regional quasi-geoid determination methods are applied, and the results are evaluated in order to identify the best and most consistent solution.

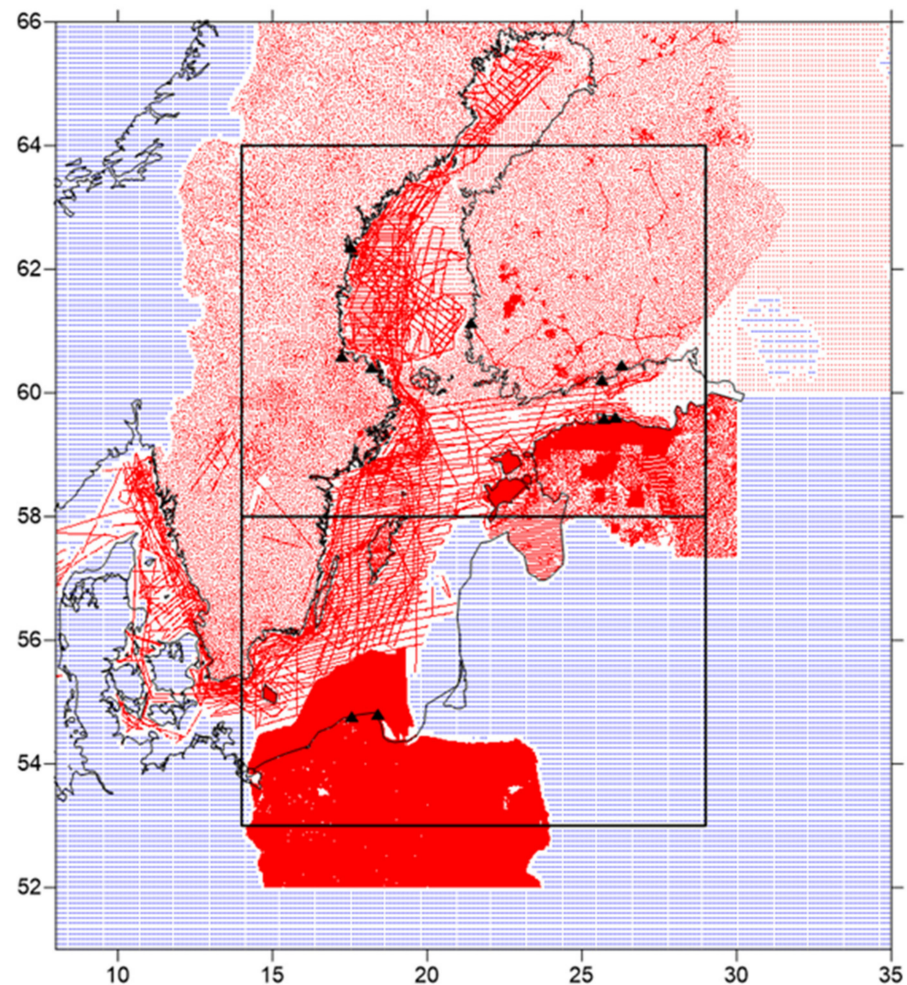


Figure 12. Gravity data selected to compute the gravimetric quasi-geoid models over the Baltic Sea test area. The data includes the gravity datasets of the NKG2015 project from Sweden, Finland, and Estonia (plus some other open datasets), new FAMOS marine gravity data from the same countries and the Polish gravity data currently in the NKG2015 gravity database. Pseudo-observations ($5' \times 5'$) generated by EIGEN-6C4 are plotted as triangles. The TG and ECR locations are plotted as black triangles. The locations of north and large quasi-geoid test areas are also illustrated.

In the LSMSA approach, the remove–compute–restore technique is applied for the gridding of the surface gravity anomaly. The RTM and EGM gravity anomaly effects are first removed from the surface gravity anomalies. The RTM effect is computed using the DEM averaged to 0.0025×0.0050 degree resolution (around 250×250 m). The residual surface gravity anomalies are then gridded using least squares collocation, as implemented in Geogrid [28]. After this, the RTM and EGM surface gravity anomaly effects are restored. This results in a surface gravity anomaly grid with 0.01×0.02 degree resolution. The LSMSA method is finally applied on this surface gravity anomaly grid using the same tuning as for the NKG2015 geoid model [22,23]. The only difference is that the satellite-only EGM and maximum degree are different.

The 3D LSC method applies the remove–compute–restore method with RTM and the EGM. An empirical covariance function is first computed for the reduced gravity anomalies, to which an analytical Tscherning and Rapp function [29] is fitted. This method is tested with the two satellite-only models mentioned above. The same DEM as for the LSMSA computations averaged to the resolution (0.0025×0.0050 degrees) is utilized. The standard IAG atmospheric correction is used [25].

In all quasi-geoid computations, the following standards are used, which are in accordance with the standards applied to the analysis of all the other observations mentioned in the previous sections. As a reference potential value (W_0), the value obtained in the NKG2015 geoid project is used ($W_0 = 62,636,858.18 \text{ m}^2/\text{s}^2$). The zero permanent tide system is used in all computations. The postglacial land uplift epoch is taken as 2000.0, which is extrapolated for the final geoid values to the mean epoch of the analysis period (2020.5) (see below).

Overall, seven gravimetric quasi-geoid models are computed. They distinguish between applying the two alternative computational approaches (LSMA or 3D LSC), the use of different background EGMs with different maximum degrees, and the application of two different solutions for the land uplift correction to be applied in order to transform the geoid solution to the epoch 2020.5, which is used for all data in this study. For the latter, either the temporal variation model for the spherical harmonic coefficients up to degree 120 from GOCO06S/ITSG-Grace2018s EGM [27,30] or the geoid uplift model NKG2016LU, which was computed by 1D Glacial Isostatic Adjustment (GIA) modeling under several assumptions [31], is used.

The relative quality of the gravimetric quasi-geoid models is evaluated using GNSS/levelling datasets from Sweden, Finland, and Estonia. All evaluations are made in a consistent way using the postglacial land uplift 2000.0 and the zero permanent tide system. Standard deviations obtained in the one-parameter GNSS/levelling fits are computed for the gravimetric quasi-geoid models. After the removal of specific country offsets, all LSMSA models and the LSC model applying a combined high resolution background EGM have a very low relative uncertainty between 1.3 and 1.5 cm standard deviation. Considering that these measures also contain errors in the GNSS and levelling observations, this is an excellent result. LSC quasi-geoid models using a satellite only EGM as background information have a significantly worse fit of 2 cm standard deviation. From these results, finally, the LSMSA quasi-geoid model using the GOCO06S satellite-only global model [27] as background and applying the land uplift correction based on the GOCO06S/ITSG-Grace2018s EGM [27,30] is chosen as the geoid model for the Baltic Sea area. Figure 13 shows the GNSS/levelling geoid residuals for the chosen model. Note that the offsets for the different countries are not subtracted yet.

The chosen quasi-geoid model is then converted to the project mean epoch 2020.5 by the land uplift correction described above. The final quasi-geoid heights at the ECR stations are summarized in Table 8.

Table 8. Final quasi-geoid heights for the Baltic Sea ECR stations at epoch 2020.5. Unit: m.

Country	ECR Station	Quasi-Geoid Height [m]
Estonia	Loksa	16.821
	Vergi	16.555
Finland	Emäsalo	15.509
	Loviisa	15.453
	Rauma	19.096
Sweden	Kobben	22.381
	Vinberget	25.065
	Mårtsbo	24.627
Poland	Władysławowo	28.883
	Łeba	30.787

The time variation of the geoid heights is very small. The geoid variations are below 0.6 mm/year for all the included TGs for both NKG2016LU [31] and GOCO06S/ITSG-Grace2018s [27,30]. This means that the time variation within the project year 2020 is well below 1 mm for all the TGs. The final geoid height time series for the TGs can thus be taken as the constant values in Table 8 (for epoch 2020.5).

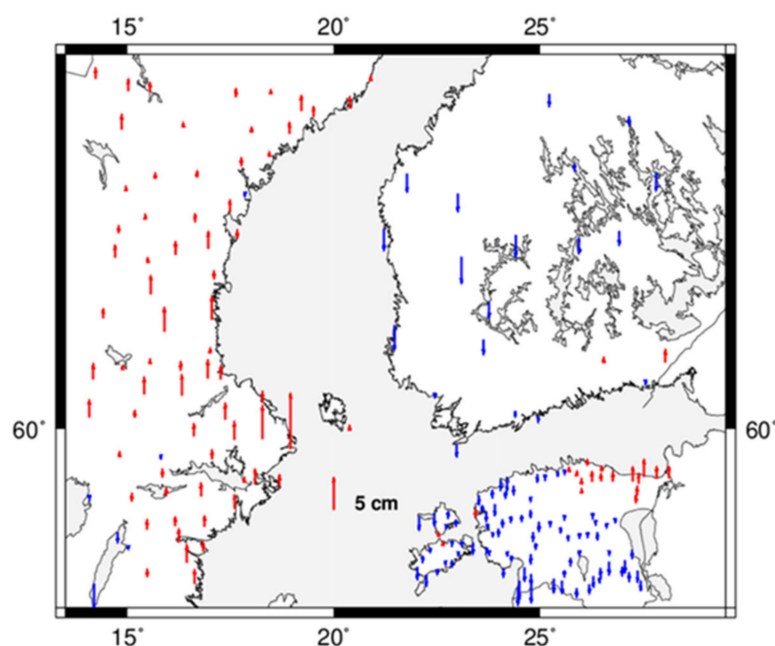


Figure 13. GNSS/levelling residuals from the 1-parameter fit of the final quasi-geoid model without corrections for specific country offsets (only one shift parameter estimated). Red arrows mean positive residuals, while blue means negative. The scale is given by the red arrow in the middle of the Baltic Sea.

2.6. Reference Frames and Joint Standards

For absolute sea level determination and height system unification, different observations such as SAR, GNSS, GOCE, terrestrial/airborne gravity data, and TGs are combined for the determination of ellipsoidal and physical heights at TG stations. In order to ensure consistent results for the different products, it is essential that any differences regarding the underlying reference frames and inconsistencies with respect to the implemented standards and models are taken properly into account. The items to be considered in this context are summarized in [1] and are not repeated here.

The standards and models used for the processing of the different observations are applied accordingly with the IERS Conventions 2010 [13]. In addition, technique-specific processing standards are applied for the individual techniques (e.g., IGS- and EPN-Standards, SAR Standards, GOCE Standards, standards for gravity, and TG data). In the previous sections, the specific standards and models are described in some detail for each observation type. These standards are consistent, such that there are no further significant error sources regarding standards and conventions, which need to be considered for their combination.

Concerning the underlying reference frames, the GNSS and SAR results are expressed in the ITRF2014, whereas the GOCE results refer to ITRF2008. The transformation parameters between both frames are rather small (max. 2.4 mm) [12], and thus, they do not need to be taken into account here.

The GNSS network stations in the Baltic Sea region are processed together with about 10 to 15 IGS/EPN stations, which are used for the datum definition of the regional network in the ITRF2014. For the processing of the GNSS solutions, the ITRF2014 station coordinates (given at the epoch 2010.0) are extrapolated over a time span of about 10 years to the observation epoch (in the year 2020) by using the ITRF2014 station velocities. To minimize the errors caused by the required extrapolation of station coordinates, stable reference stations with a long observation time span are selected for the realization of the geodetic datum. As an example, Figure 14 shows the time series of the IGS/EPN station Metsähovi in Finland. The observation time series of about 25 years indicates a high long-term stability, so that the extrapolation of station coordinates from epoch 2010.0 to the year 2020.5 can be

performed with a sufficient accuracy. The vertical station velocity of about 4 mm/year with respect to ETRF2014 and IGB14 reference frames can be well explained by postglacial uplift.



Figure 14. Residual position time series of GNSS station Metsähovi in Finland [Source: EPN website at https://www.epncb.oma.be/_productsservices/timeseries/ (accessed on 17 May 2022)].

In the context of the extrapolation of station positions and the transformation of GNSS and SAR solutions into ITRF2014, possible non-linear station motions may also affect the results. As shown, for example, in Figure 14, the amplitudes of the annual signals are mostly in the range of a few millimeters only, and thus, they can be neglected in the framework of this analysis.

Furthermore, in principle, the time variability of the center of mass (CM) versus the center of figure (CF) is an issue that has to be considered as well, since the geometric quantities are expressed in the CF frame, whereas the gravimetric quantities refer to CM. The ITRF2014 provides an annual geocenter model with amplitudes of 2.6 mm, 2.9 mm, and 5.7 mm for the x -, y -, and z -component, respectively [12]. So, in principle, these corrections could be applied for the combination of geometric and gravimetric observations, but with respect to the current accuracy level of the obtained SAR positions, the geocenter variations can be neglected.

3. Absolute Sea Level and Height System Unification

3.1. Absolute Height Experiments

The heights obtained from the individual observation techniques are summarized for the static case in Table 9 (refer to Table 4 for ECR ellipsoidal heights, Table 6 for GNSS ellipsoidal heights, Table 7 for TG heights). Static here means that either average values over the observation period of the year 2020 are considered (ECR, quasi-geoid and TG heights) or that coordinates are transformed to epoch 2020.5 (GNSS). As it is shown in Section 2.1, the accuracy of the SAR positions, which, on average, is at the level of a decimeter (see Table 5), is not yet sufficient to observe time variations of ellipsoidal heights over the period of one year. Therefore, coordinate variations within the year 2020 are not further considered.

Table 9. Summary of observed ellipsoidal, geoid and TG heights at Baltic Sea network. All heights represent mean values averaged over the observation period in year 2020 or for epoch 2020.5. h^{ECR} : ellipsoidal height of ECR reference point; N^{TG}, N^{ECR} : quasi-geoid height at location (same for tide gauge and ECR); z^{TG} : TG sea level height above zero marker; h^{GNSS} : ellipsoidal height of GNSS reference point.

ECR Station	Local Tie	h^{ECR} Ellipsoidal Height [m]	$N^{TG} = N^{ECR}$ Geoid Height [m]	z^{TG} Tide Gauge [m]	h^{GNSS} Ellipsoidal Height [m]
Władysławowo	TG, GNSS	+34.640	+28.883	+0.253	+34.758
Łeba	TG, GNSS	+34.389	+30.787	+0.224	+37.886
Vergi	GNSS	+28.966	+16.555	n/a	+30.069
Loksa	TG	+20.076	+16.821	+0.343	n/a
Emäsalo	TG	+34.293	+15.509	+0.338	n/a
Loviisa	GNSS	+46.840	+15.453	n/a	+49.879
Rauma	TG	+24.082	+19.096	+0.258	n/a
Kobben	TG	+25.659	+22.381	+0.188	n/a
Mårtsbo	GNSS	+75.477	+24.627	n/a	+75.558
Vinberget	TG, GNSS	+149.654	+25.065	+0.175	+150.206

In order to connect the ECR reference point either to the TG zero marker or the GNSS reference point, conventional spirit levelling campaigns between the TG and the ECR and/or the GNSS and the ECR reference point are performed by the station operators. The results of the local ties are summarized in Table 10.

Table 10. Levelled height differences between ECR reference point and the TG or GNSS reference points. Δh_{ECR}^{TG} : ellipsoidal height difference from ECR reference point to TG zero marker; Δh_{GNSS}^{ECR} : ellipsoidal height difference from GNSS reference point to ECR reference point.

ECR Station	Local Tie	Δh_{ECR}^{TG} ECR to Tide Gauge [m]	Δh_{GNSS}^{ECR} GNSS to ECR [m]
Władysławowo	TG	−5.638	n/a
Władysławowo	GNSS	n/a	−0.135
Łeba	TG	−3.049	n/a
Łeba	GNSS	n/a	−3.932
Vergi	GNSS	n/a	−0.996
Loksa	TG	−2.639	n/a
Emäsalo	TG	−17.816	n/a
Loviisa	GNSS	n/a	−3.574
Rauma	TG	−5.007	n/a
Kobben	TG	−2.961	n/a
Mårtsbo	GNSS	n/a	−0.032
Vinberget	TG	−123.523	n/a
Vinberget	GNSS	n/a	−0.998

For the ECR stations co-located to a permanent GNSS station, the resulting heights can be directly compared by applying the relative height difference between the GNSS antenna reference point and the ECR reference point. This is an indicator about the absolute performance of the SAR positioning technique. Table 11 (right column) shows the results of this comparison. It can be identified that the absolute height differences between the two techniques are varying, and that no ultimate conclusion can be drawn from this comparison. While three stations exhibit good to reasonable agreement between GNSS and ECR heights at decimeter level or better, for three other stations, height differences are at a level of several decimeters up to half a meter. As one can assume that the GNSS derived heights are accurate at a level of a few centimeters, the ECR-derived heights are the main driver for the absolute performance results. Regarding the reason why some ECR positioning results are better than others, there is no unique answer. For the station Vinberget, the reason could be

that the observation time series is relatively short, but for the stations in Loviisa and Łeba, the raw observation data series seem to be good, and no indicator about possible problems can be identified.

Table 11. Comparison of SAR positioning heights at ECR stations to co-located permanent GNSS station heights. $h_{comp}^{ECR} = h^{GNSS} + \Delta h_{GNSS}^{ECR}$: ellipsoidal height transferred from GNSS to ECR station; Δh^{ECR} : ellipsoidal height difference transferred GNSS versus ECR.

ECR Station	h_{comp}^{ECR} Computed Ell. Height [m]	h^{ECR} Observed Ell. Height [m]	Δh^{ECR} Computed-Observed [m]
Władysławowo	+34.623	+34.640	−0.017
Łeba	+33.954	+34.389	−0.435
Vergi	+29.073	+28.966	+0.107
Loviisa	+46.305	+46.840	−0.535
Mårtsbo	+75.526	+75.477	+0.049
Vinberget	+149.208	+149.654	−0.446

Average physical heights (for the year 2020) of TG stations H^{TG} referring to a unique reference equipotential surface and not considering the absolute or relative sea level are computed from the ECR ellipsoidal height, the local tie between the ECRs and the TGs, and the quasi-geoid height with $H^{TG} = h^{ECR} + \Delta h_{ECR}^{TG} - N^{TG}$. The results are provided in Table 12 (middle column).

Table 12. Physical heights H^{TG} of TG stations as computed from the ECR ellipsoidal height, the local tie from the ECR to the TG and the quasi-geoid height. Absolute sea level heights S^{TG} from physical heights and tide gauge readings.

ECR Station	H^{TG} Physical Height [m]	S^{TG} Absolute Sea Level [m]
Władysławowo	+0.119	+0.372
Łeba	+0.553	+0.777
Loksa	+0.616	+0.959
Emäsalo	−0.032	+0.306
Rauma	−0.021	+0.237
Kobben	+0.317	+0.505
Vinberget	+1.066	+1.241

As all TG zero markers refer to the same vertical reference system (EVRS), meaning, that in the ideal case, this height for all stations shall be zero, any deviation from zero can be interpreted as a performance indicator for the involved quantities and, here, mainly the performance of the SAR positioning. The results show that some stations seem to provide very good results with only a few centimeters offset, while other stations exhibit an offset of several decimeters up to a meter. Regarding the results of the SAR positioning, there seems to be some correlation of the physical height results with the SAR observation quality, the SAR residuals, and the length of the SAR observation time series. For example, the stations Emäsalo and Rauma have a better performance than some other stations. The time series of Vinberget is very short, and therefore, the uncertainty is probably significantly larger. For the stations Władysławowo, Łeba, Loksa, and Kobben, there is a larger variability in the SAR observation quality, which could be the reason for higher uncertainties. At this point, it is difficult to provide a complete assessment of the results, as no single reason can be identified.

From the TG physical heights, it is then easy to compute the absolute sea level height by adding the averaged tide gauge records $S^{TG} = H^{TG} + z^{TG}$. The results are shown in Table 12 (right column). These results contain the full uncertainty of the physical heights of

the TG stations and consequently the uncertainties of the ECR ellipsoidal heights. Therefore, all what is said above also applies to the absolute sea level heights.

3.2. Baseline (Relative) Height Experiments

Relative height differences are compared between GNSS or TG stations and those observed with the ECRs. There are several of such baselines available, which can be observed over long or short distances. For the relative comparisons between station A and station B, the following equations are applied.

$$\begin{aligned} \Delta h^{GNSS-A/B} &= h^{GNSS-B} - h^{GNSS-A} \\ \Delta h^{ECR-A/B} &= \left(h^{ECR-B} - \Delta h_{GNSS-B}^{ECR-B} \right) - \left(h^{ECR-A} - \Delta h_{GNSS-A}^{ECR-A} \right) \\ \Delta \Delta h^{(GNSS-A/B)-(ECR-A/B)} &= \Delta h^{GNSS-A/B} - \Delta h^{ECR-A/B} \end{aligned}$$

The baseline comparisons provided in Table 13 again show diverse results. Basically, the differences between GNSS and ECR observed height differences vary between a few centimeters and some decimeters. For stations that exhibit a large absolute offset (see Table 11, stations Łeba, Loviisa, Vinberget) the differential height error between these stations becomes small (below a decimeter), while the differential error between one of these stations with the other stations becomes significantly larger. This indicates that there is a systematic height offset in the ECR positioning results with the same sign, as it is also shown in the absolute comparisons in Table 11. The reason for this is yet unknown. The situation is similar for the stations that exhibit a small absolute offset (see Table 11, stations Władysławowo, Vergi, Mårtsbo), the differential height error between these stations becomes also small (below a decimeter). This indicates that the internal accuracy of the ECR heights seem to be good, but that systematic offsets between the instruments are present.

Table 13. Relative (baseline) height differences between ECR stations A and B and co-located GNSS stations A and B and differences of the baseline height differences. GNSS height differences and ECR height differences transferred to the GNSS reference markers are computed with the equation above.

Station A	Station B	$\Delta h^{GNSS-A/B}$ Ell. Height Difference [m]	$\Delta h^{ECR-A/B}$ Ell. Height Difference [m]	$\Delta \Delta h^{(GNSS-A/B)-(ECR-A/B)}$ Double Difference Ell. Height [m]
Władysławowo	Łeba	+3.128	+3.546	−0.418
Władysławowo	Vergi	−4.689	−4.813	+0.124
Władysławowo	Loviisa	+15.121	+15.639	−0.518
Władysławowo	Mårtsbo	+40.800	+40.734	+0.066
Władysławowo	Vinberget	+115.448	+115.877	−0.429
Łeba	Vergi	−7.817	−8.359	+0.542
Łeba	Loviisa	+11.993	+12.093	−0.100
Łeba	Mårtsbo	+37.672	+37.188	+0.484
Łeba	Vinberget	+112.320	+112.331	−0.011
Vergi	Loviisa	+19.810	+20.452	−0.642
Vergi	Mårtsbo	+45.489	+45.547	−0.058
Vergi	Vinberget	+120.137	+120.690	−0.553
Loviisa	Mårtsbo	+25.679	+25.095	+0.584
Loviisa	Vinberget	+100.327	+100.238	+0.089
Mårtsbo	Vinberget	+74.648	+75.143	−0.495

Finally, as another relative height experiment, the sea level at tide gauge stations can be compared. For the relative comparisons between tide gauge station A and station B, the following equations are applied.

$$\begin{aligned} \Delta z^{TG-A/B} &= z^{TG-B} - z^{TG-A} \\ \Delta S^{TG-A/B} &= S^{TG-B} - S^{TG-A} \\ \Delta \Delta S^{TG-A/B} &= \Delta z^{TG-A/B} - \Delta S^{TG-A/B} \end{aligned}$$

The results from the tide gauge baseline differences presented in Table 14 show, in most cases, large differences. Right now, it seems that only three ECR stations with good performance and linked to a tide gauge are available. These are the stations in Władysławowo (see also comment above for GNSS comparisons), Emäsalo, and Rauma, where differences up to a decimeter can be achieved. There is also a good agreement between Łeba and Loksa, which is probably due to similar systematic offsets at both stations (see again comment above for GNSS comparisons).

Table 14. Relative (baseline) height differences between ECR stations A and B and between co-located TG stations A and B and differences of baseline height differences. TG height differences and ECR height differences transferred to the TG reference markers are computed with the equation above.

Station A	Station B	$\Delta z^{TG-A/B}$ Tide Gauge Height Difference [m]	$\Delta S^{TG-A/B}$ Absolute Sea Level Height Difference [m]	$\Delta\Delta S^{TG-A/B}$ Double Difference Sea Level [m]
Władysławowo	Łeba	−0.029	+0.405	−0.434
Władysławowo	Loksa	+0.090	+0.587	−0.497
Władysławowo	Emäsalo	+0.085	−0.066	+0.151
Władysławowo	Rauma	+0.005	−0.135	+0.140
Władysławowo	Kobben	−0.065	+0.133	−0.198
Władysławowo	Vinberget	−0.078	+0.869	−0.947
Łeba	Loksa	+0.119	+0.182	−0.063
Łeba	Emäsalo	+0.114	−0.471	+0.585
Łeba	Rauma	+0.034	−0.540	+0.574
Łeba	Kobben	−0.036	−0.272	+0.236
Łeba	Vinberget	−0.049	+0.464	−0.513
Loksa	Emäsalo	−0.005	−0.653	+0.648
Loksa	Rauma	−0.085	−0.722	+0.637
Loksa	Kobben	−0.155	−0.454	+0.299
Loksa	Vinberget	−0.168	+0.282	−0.450
Emäsalo	Rauma	−0.080	−0.069	−0.011
Emäsalo	Kobben	−0.150	+0.199	−0.349
Emäsalo	Vinberget	−0.163	+0.935	−1.098
Rauma	Kobben	−0.070	+0.268	−0.338
Rauma	Vinberget	−0.083	+1.004	−1.087
Kobben	Vinberget	−0.013	+0.736	−0.749

4. Data and Products, Summary and Conclusions, Future Work

4.1. Data and Products

All data and products resulting from this work are publicly available at the web site: <https://www.asg.ed.tum.de/iapg/baltic/> (accessed on 17 May 2022). At this website, supplementary information is also available, which provides detailed data descriptions and reports describing the procedures and intermediate results. Basically, the complete data analysis requires various intermediate processing steps, which are described in [1] and applied to the data of the year 2020. Table 15 summarizes the content of the data files, which formed the basis for all the results presented in Sections 2 and 3.

The SAR data analysis and value adding processor generates the raw azimuth and range observations for the observed ECR locations by point target image analysis. Before these raw observations may be used for position estimation, they need to be corrected for environmental, geophysical, and instrumental effects (for more details, refer to [1]). The various corrections are computed in terms of azimuth and range corrections and are stored in different products. The results of the SAR positioning include target coordinates in ITRF2014 and their uncertainties derived from the variance–covariance matrix. Coordinates and heights determined from GNSS positioning, TG data analysis, and geoid computations are stored as average values in the products. The same is true for the resulting physical heights and absolute sea level heights at TG stations.

Table 15. Summary of data and products.

Product Title	Product Description	Section
SAR Target Locations (PTA-RES)	Target range and azimuth location(s) from point target analysis.	Section 2.1
SAR Raw Measurements (PTA-OBS)	SAR observation file generated from the point target analysis file. Processor specific corrections are applied to range and azimuth.	Section 2.1
SAR Tropospheric Delays (COR-TD)	Tropospheric delays stored as one-way path delay in units of meters.	Section 2.1
SAR Ionospheric Delay (COR-ID)	Ionospheric delays stored as one-way path delay in units of meters.	Section 2.1
Geodynamic Corrections (COR-GC)	Geodynamic corrections to SAR range and azimuth observations due impact of solid Earth tidal deformations, ocean loading, atmospheric pressure loading, rotational deformation due to polar motion, ocean pole tide loading and secular trends.	Section 2.1
Sentinel-1 Systematic Effects (COR-SC)	Sensor specific calibration constants and corrections to be applied to raw range and azimuth observations.	Section 2.1
ECR Phase Center (COR-EC1)	Phase center shift of the ECR due to orbit geometry to be added as a correction to the observations.	Section 2.1
ECR Electronic Delay (COR-EC2)	ECR electronics causes a signal delay to be corrected in the SAR measurements.	Section 2.1
SAR Positions (SAR-POS)	Time series of coordinates of the SAR target as X, Y, Z coordinates in the ITRF2014 and uncertainties.	Section 2.2
SAR Observation Residuals (SAR-OBS)	Time series of range and azimuth standard deviations and observation residuals.	Section 2.2
GNSS Positions (GNSS-POS)	Coordinates of the GNSS stations as X, Y, Z coordinates in the ITRF2014 and uncertainties.	Section 2.3
Sea Surface Height at TG (TG-SSH)	Corrected sea surface heights observed at TG with respect to TG benchmark.	Section 2.4
Geoid Heights (GEO-HGT)	Geoid heights with mean epoch 2020.5 for the tide gauge stations.	Section 2.5
Tide Gauge Heights (TG-HGT)	Average of unified physical heights of tide gauge stations.	Section 3.1
Absolute Sea Level Heights (SL-ABS)	Average of absolute sea level heights of tide gauge stations.	Section 3.1

4.2. Summary and Conclusions

The achieved results, in the context of the project goal, namely to compute absolute sea level heights and to enable height unification in the Baltic Sea area, are summarized in the following paragraphs, and some conclusions are drawn.

First, the feasibility of using ECRs as a new observation tool to determine and monitor geometric 3D positions is assessed with regard to their operability and calibration. Compared to passive CRs with trihedral triangular shape with 1.5 m inner leg length, the ECR exhibits considerable advantages regarding transport, ease of installation, and strength

of backscattered signal for both ascending and descending tracks. Comparable passive infrastructure would have required two CRs at each station and more elaborate mounting solutions to support the bulky and heavy reflectors. The small and relatively lightweight ECRs can be attached to existing infrastructures, e.g., the masts supporting GNSS antennas, or new platforms can be set up with reasonable efforts. However, because these are active electronic devices, there are some disadvantages as well, which are mostly related to power supply, reliability in all weather conditions, electronic delays and phase center stability, and acquiring radio licenses. During long-term operations of the ECRs, it turned out that the maintenance of several devices was needed more often than planned. This was because of electronic failure due to water intrusion (deteriorated sealing of ECR housings), because of time keeping problems of the ECRs via GNSS, which can yield corrupted dates leading to missed activations, and because of interrupted remote access to the ECRs via internet. Electronic delays need to be considered during data processing and requires calibration parameters. Initially, it was assumed that the electronic delay per pass geometry is identical for all ECRs of the same design and can be determined on the calibration site in Oberpfaffenhofen, Germany, but from the results obtained in the Baltic Sea test network, there are indications that each ECR somehow has its own characteristics, and individual calibration sessions need to be performed before installing them at the target locations.

The SAR positioning results are critically assessed in terms of internal and external uncertainties. The majority of ECRs are installed at locations with low background clutter, and the signals are very reliably detected in the acquired Sentinel-1 SAR image data. Phase center corrections for ascending and descending orbits as well as for different incidence angles are applied before all range and azimuth raw observations go through an outlier detection process. From the positioning results, it can be identified that monthly solutions are the shortest time interval in order to compute realistic ellipsoidal coordinates. At most ECR stations, only 10 valid range and 10 valid azimuth observations are collected over a period of one month, which is the minimum for a stable performance of the positioning processor. With more observations, the positioning becomes more stable for most stations. As a promising result, it can be stated that the SAR positioning exhibits high internal accuracies. The internal accuracies for the solutions across all stations vary between few centimeters down to millimeters in the local north, east, and height topocentric frame. This implies that with a continuous observation period with good data coverage, relative coordinate variations can be observed on bi-monthly (monthly, under optimal conditions) time intervals with a few centimeters' accuracy. For absolute position accuracy, however, a well-calibrated and long-term stable instrument is needed.

GNSS data processing is performed as daily network solutions in the double-difference mode. ITRF2014 is used as the reference frame, in which all IGS global products are available for the calculations: precise orbits, the Earth's rotation parameters, and the corrections of GNSS satellite clocks. Based on these solutions, the time series of Cartesian coordinates covering the entire year 2020 are generated. The final average coordinate solutions for all stations are computed as 3D Cartesian Coordinates in ITRF2014 and as ellipsoidal coordinates referred to the GRS-80 ellipsoid for epoch 2020.50. The internal accuracy of the determined coordinates is at the level of a (sub-)millimeter, which is, by far, sufficient to reach the envisaged goals at a level of one centimeter.

TG data processing follows the existing standard approaches. The resulting annual mean sea level estimates are comparable to other concurrent tide gauge processing approaches. The consistency of the TG time series for the Baltic Sea test network is achieved by a rigorous conversion into the common vertical datum and accounting for the vertical land motion. The used TG sensor technologies all assured centimeter accuracy for the resulting tide gauge records. It is shown that consistency (e.g., a reduction to the same time epoch, a common vertical datum, the removal of land-uplift effects, tide gauge connections with national geodetic infrastructure) is essential for achieving geodetic accuracy required for combination with other sensors.

Several regional geoid models applying different procedures are computed, and they all agree very well with each other. The final geoid model for the Baltic Sea area is converted to mean epoch 2020.5 by applying land uplift correction. As can be judged from the comparison to GNSS/levelling, the standard uncertainty of the geoid heights is estimated to be approximately 1 cm in a relative sense. All data are processed with the same standards and conventions in order to keep compatibility with the other observations. The time variation of the geoid heights is very small (0.6 mm/year) for all TG stations. Therefore, the final geoid height time series for the TG stations is taken as the constant values for epoch 2020.5.

For the combination of the different geometric and gravimetric quantities, a correct treatment of the permanent tide and a consistent correction of postglacial uplift is essential to achieve consistent results. Regarding the extrapolation of ITRF2014 station positions, stable reference frame stations are selected to ensure that linear propagation models provide sufficiently accurate results. The transformation parameters between ITRF2014 and ITR2008 and the geocenter variations are neglected, as the effects are much below the centimeter level. The same holds for non-linear motions in station positions. However, if GNSS solutions computed in the ITRF2014 are compared with EPN results, the transformation formulae between the ITRS and ETRS89 need to be applied, since the effect is about 75 cm for observations in the year 2020. All these items are carefully considered when processing the individual data sets. In conclusion, no systematic effects related to references frames and processing standards are present in the unified heights and absolute sea level results.

The results of the individual observations techniques in terms of heights are combined for the static case. Static here means that average values over the observation period of the year 2020 are considered, disregarding sub-annual variations of heights. The reason for this is that the weakest point is the accuracy of the SAR positions, which, on average, is at a level of a decimeters (for a few good stations).

For the ECR stations co-located to a permanent GNSS station, the resulting heights can be directly compared by taking into account the local tie measurements in order to quantify the absolute performance of the SAR positioning technique. As the results are varying, no ultimate conclusion can be drawn from this comparison. While three stations exhibit good to reasonable agreement at decimeter level or below, for three other stations, differences are at a level of several decimeters up to half a meter. Regarding the reason why some ECR positioning results are better than others, there is no unique answer. It is assumed that an insufficient electronic calibration of the ECRs and/or possible instabilities of the calibration parameters, as discussed above, are responsible.

From the ECR stations co-located at a tide gauge station, the resulting physical heights of the tide gauge zero markers above the reference equipotential surface (GOC-based geoid) are computed. As all tide gauge zero markers are already provided in the EVRS, meaning that, in the ideal case, this height for all stations shall be zero, any deviation from zero can be interpreted as a performance indicator for the involved quantities and, here, mainly the performance of the SAR positioning. The results show that some stations seem to provide very good results with only a few centimeters offset, while other stations exhibit an offset of several decimeters up to a meter. These results need to be further analyzed together with the performance of the individual ECR stations and with respect to the length of the data time series. Regarding the results, there seems to be some correlation of the physical height results with the SAR observation quality, the SAR residuals, and the length of the SAR observation time series. At this point, it is difficult to provide a complete assessment of the results, as no single reason can be identified, before the ECR calibration performance can be checked in detail.

For linking tide gauge stations to the permanent GNSS network via ECR stations, baseline height differences between ECRs collocated to GNSS stations and between ECRs collocated to tide gauge stations are computed. The results of the baseline comparisons again show a diverse behavior. Basically, the differences between GNSS and ECR observed height differences vary between a few centimeters and some decimeters. For stations that

exhibit a large absolute offset, the differential height error between these stations becomes small (below a decimeter), while the differential error between one of these stations with the other stations becomes significantly larger. This indicates that there is a systematic height offset in the ECR positioning results with the same sign, as it is also identified in the absolute comparisons. Similarly, for stations that exhibit a small absolute offset, the differential height error between these stations also becomes small (below a decimeter). Right now, it seems that only two ECR stations (Emäsalo, Rauma) with good performance and linked to a tide gauge are available, where differences up to a decimeter can be achieved. There is also good agreement between two stations with similar systematic offsets at both stations. This could hint towards a better relative performance if absolute errors can be eliminated by differentiation. This is only true if the absolute calibration is stable in time, which is not guaranteed when looking to all results obtained from the SAR positioning.

4.3. Future Work

From the scientific point of view, the achieved results are not fully satisfactory, as there remain too many uncertainties with respect to the performance of the ECRs and specifically with respect to the instrument calibration. However, it clearly showed the potential of the method, a way to develop the technique in future, and a lot of detailed information on how to improve the data processing. ECRs can provide additional information for areas of no previous geodetic position observations but cannot replace current GNSS positioning techniques. The design of the ECRs needs to be improved in order to enable remote unmanned operations in harsh environmental conditions. Specifically, the calibration and characterization of the electronics needs to be improved before these instruments can meet geodetic accuracy requirements.

As a result, it is identified that ECRs are not suitable to observe temporal coordinate variations with amplitudes up to a centimeter and with shorter temporal resolution than a month. However, they can be used for observations of large movement (>decimeter/month) in areas with critical slopes undergoing landslides, for volcanos and fast subsidence, e.g., dolines or cave collapses. Additionally, ECRs might be a tool to absolute reference coordinates in order to fix the datum of SAR interferometry results.

Well-calibrated ECRs co-located with GNSS also can provide additional data for local deformation monitoring at the site, 3D absolute positioning, and atmospheric studies and can be compared with GNSS data and time series in the long run. In addition, ECRs as artificial persistent scatters co-located with GNSS permanent stations can be useful for the future calibration of European ground motion service (EGMS) products and to transform the deformation maps and rates into a global reference frame.

Within the project, a very valuable data set has been compiled, which offers the possibility to enhance methods and procedures in order to develop the SAR positioning technique towards operability. All data are publicly available and can be used for further detailed analyses.

Author Contributions: Conceptualization, T.G.; Data curation, A.E. (Artu Ellmann), C.G., L.J., S.M., F.N., A.E. (Andreas Engfeldt), T.K., T.S., M.N., M.S., A.Š., S.V. and R.Z.; Methodology, T.G., J.Å., D.A., A.E. (Artu Ellmann), C.G., J.N. and M.P.; Project administration, T.G.; Resources, A.E. (Andreas Engfeldt), C.G., L.J., S.M., F.N., T.S., A.Š., S.V. and R.Z.; Software, M.S.; Writing—original draft, T.G., J.Å., D.A., A.E. (Artu Ellmann), C.G., J.N., M.P. and R.Z. All authors have read and agreed to the published version of the manuscript.

Funding: This research partially was funded by European Space Agency (ESA), grant number 4000126830/19/I-BG. Tallinn University of Technology research is partly funded by the Estonian Science Council grant PRG330. The APC was funded by the University Library of Technical University of Munich via the Open-Access publication fund.

Data Availability Statement: All data and results as well as detailed reports can be downloaded at: <https://www.asg.ed.tum.de/iapg/baltic/> (accessed on 17 May 2022).

Acknowledgments: Apart from the authors, the following people from the contributing institutions supported the local installation of the ECRs: Markus Heinze (TUM), Adam Lyszkowicz (CBK-PAN), and Janusz B. Zielinski (CBK-PAN). In addition, the authors acknowledge the support of the following agencies and institutions: The Geodesy department of the Estonian Land Board is thanked for the installation assistance of the Estonian ECR sites.

Conflicts of Interest: The authors declare no conflict of interest.

References

1. Gruber, T.; Ågren, J.; Angermann, D.; Ellmann, A.; Engfeldt, A.; Gisinger, C.; Jaworski, L.; Marila, S.; Nastula, J.; Nilfouroushan, F.; et al. Geodetic SAR for Height System Unification and Sea Level Research—Observation Concept and Preliminary Results in the Baltic Sea. *Remote Sens.* **2020**, *12*, 3747. [CrossRef]
2. Gisinger, C.; Balss, U.; Pail, R.; Zhu, X.X.; Montazeri, S.; Gernhardt, S.; Eineder, M. Precise Three-Dimensional Stereo Localization of Corner Reflectors and Persistent Scatterers with TerraSAR-X. *IEEE Trans. Geosci. Remote Sens.* **2015**, *53*, 1782–1802. [CrossRef]
3. Bourbigot, M.; Johnsen, H.; Piantanida, R.; Sentinel-1 Product Definition. Technical Note by Sentinel-1 Mission Performance Center (MPC), Doc. S1-RS-MDA-52-7440, Iss. 2, Rev. 6, Date 22 July 2015. Available online: https://sentinels.copernicus.eu/web/sentinel/user-guides/sentinel-1-sar/document-library/-/asset_publisher/1dO7RF5fjMbd/content/sentinel-1-product-definition (accessed on 17 May 2022).
4. Potin, P.; Gascon, F.; Stromme, A.; Zehner, C.; Wilson, H.; Figa, J.; Obligis, E.; Lindstrot, R. *Sentinel High Level Operations Plan*; ESA Technical Note, COPE-SIOP-EOPG-PL-15-0020, iss. 3, rev. 1; ESA: Frascati, Italy, 2021.
5. Gisinger, C.; Schubert, A.; Breit, H.; Garthwaite, M.; Balss, U.; Willberg, M.; Small, D.; Eineder, M.; Miranda, N. In-Depth Verification of Sentinel-1 and TerraSAR-X Geolocation Accuracy using the Australian Corner Reflector Array. *IEEE Trans. Geosci. Remote Sens.* **2021**, *59*, 1154–1181. [CrossRef]
6. Cumming, I.G.; Wong, F.H. *Digital Processing of Synthetic Aperture Radar Data*; Artech House: London, UK, 2005; ISBN 978-1-58053-058-3.
7. Miranda, N.; Meadows, P.J. *Radiometric Calibration of S-1 Level-1 Products Generated by the S-1 IPF*; ESA Technical Document, Doc. ESA-EOPG-CSCOP-TN-0002, Iss. 1.0, Date 21 May 2015; ESA: Frascati, Italy, 2015.
8. Schubert, A.; Miranda, N.; Geudtner, D.; Small, D. Sentinel-1A/B Combined Product Geolocation Accuracy. *Remote Sens.* **2017**, *9*, 607. [CrossRef]
9. Hajduch, G.; Vincent, P.; Cordier, K.; Grignoux, M.; Husson, R.; Peureux, C.; Piantanida, R.; Recchia, A.; Francheschi, N.; Schmidt, K.; et al. *S-1A & S-1B Annual Performance Report 2020*; ESA Technical Document, Doc. MPC-0504, Iss. 1.1, Date 16 March 2021; ESA: Frascati, Italy, 2021.
10. Czikhhardt, R.; van der Marel, H.; Papco, J.; Hanssen, R.F. On the Efficacy of Compact Radar Transponders for InSAR Geodesy: Results of Multiyear Field Tests. *IEEE Trans. Geosci. Remote Sens.* **2022**, *60*, 1–13. [CrossRef]
11. Dach, R.; Lutz, S.; Walser, P.; Fridez, P. (Eds.) *Bernese GNSS Software Version 5.2. User Manual*; Astronomical Institute, University of Bern, Bern Open Publishing: Bern, Switzerland, 2015; ISBN 978-3-906813-05-9. [CrossRef]
12. Altamimi, Z.; Rebischung, P.; Metivier, L.; Collilieux, X. ITRF2014: A new release of the International Terrestrial Reference Frame modeling nonlinear station motions. *J. Geophys. Res. Solid Earth* **2016**, *121*, 6109–6131. [CrossRef]
13. Petit, G.; Luzum, B. (Eds.) *IERS Conventions 2010. 20210*, Verlag des Bundesamts für Kartographie und Geodaesie. Available online: <https://iers-conventions.obspm.fr/> (accessed on 17 May 2022).
14. Varbla, S.; Ågren, J.; Ellmann, A.; Poutanen, M. Treatment of tide gauge time series and marine GNSS measurements for vertical land motion with relevance to the implementation of the Baltic Sea Chart Datum 2000. *Remote Sens.* **2022**, *14*, 920. [CrossRef]
15. Moritz, H. *Advanced Physical Geodesy*; Wichmann; Abacus Press: Karlsruhe, Germany; Tunbridge, UK, 1980; ISBN 978-3-87907-106-7.
16. Tscherning, C.; Rapp, R.H. *Closed Covariance Expressions for Gravity Anomalies, Geoid Undulations, and Deflections of the Vertical Implied by Anomaly Degree Variance Models*; Report No. 208; Dep. Geod. Sci. Ohio State University: Columbus, OH, USA, 1974.
17. Tscherning, C.C. Geoid Determination by 3D Least-Squares Collocation. In *Geoid Determination: Theory and Methods*; Sansò, F., Sideris, M.G., Eds.; Lecture Notes in Earth System Sciences; Springer: Berlin/Heidelberg, Germany, 2013; pp. 311–336. ISBN 978-3-540-74700-0.
18. Forsberg, R. *A Study of Terrain Reduction, Density, Anomalies and Geophysical Inversion Methods in Gravity Field Modeling*; Dep. Geod. Sci. Ohio State University: Columbus, OH, USA, 1984.
19. Sjöberg, L. Refined least squares modification of Stokes' formula. *Manuscr. Geod.* **1991**, *16*, 367–375.
20. Sjöberg, L.E.; Bagherbandi, M. (Eds.) *Gravity Inversion and Integration—Theory and Applications in Geodesy and Geophysics*; Springer International Publishing: Cham, Switzerland, 2017; ISBN 978-3-319-50298-4.
21. Ågren, J.; Sjöberg, L.E.; Kiamehr, R. The new gravimetric quasigeoid model KTH08 over Sweden. *J. Appl. Geod.* **2009**, *3*, 143–153. [CrossRef]
22. Ågren, J.; Strykowski, G.; Bilker-Koivula, M.; Omang, O.; Mårdla, S.; Forsberg, R.; Ellmann, A.; Oja, T.; Liepins, I.; Parseliunas, E.; et al. The NKG2015 gravimetric geoid model for the Nordic-Baltic region. In Proceedings of the 1st Joint Commission 2 and IGFS Meeting International Symposium on Gravity, Geoid and Height Systems, Thessaloniki, Greece, 19–23 September 2016. Available online: https://www.isgeoid.polimi.it/Geoid/Europe/NordicCountries/GGHS2016_paper_143.pdf (accessed on 17 May 2022).

23. Märdla, S.; Ågren, J.; Strykowski, G.; Oja, T.; Ellmann, A.; Forsberg, R.; Bilker-Koivula, M.; Omang, O.; Paršeliūnas, E.; Liepinš, I.; et al. From Discrete Gravity Survey Data to a High-resolution Gravity Field Representation in the Nordic-Baltic Region. *Mar. Geod.* **2017**, *40*, 416–453. [[CrossRef](#)]
24. Förste, C.; Bruinsma, S.L.; Abrykosov, O.; Lemoine, J.-M.; Marty, J.C.; Flechtner, F.; Balmino, G.; Barthelmes, F.; Biancale, R. EIGEN-6C4 the latest combined global gravity field model including GOCE data up to degree and order 2190 of GFZ Potsdam and GRGS Toulouse. *GFZ Data Serv.* **2014**. [[CrossRef](#)]
25. Moritz, H. Geodetic Reference System 1980. *J. Geod.* **2000**, *74*, 128–162. [[CrossRef](#)]
26. Förste, C.; Abrykosov, O.; Bruinsma, S.; Dahle, C.; König, R.; Lemoine, J.-M. ESA's Release 6 GOCE gravity field model by means of the direct approach based on improved filtering of the reprocessed gradients of the entire mission. *GFZ Data Serv.* **2019**. [[CrossRef](#)]
27. Kvas, A.; Mayer-Gürr, T.; Krauss, S.; Brockmann, J.M.; Schubert, T.; Schuh, W.-D.; Pail, R.; Gruber, T.; Jäggi, A.; Meyer, U. The satellite-only gravity field model GOCO06s. *GFZ Data Serv.* **2019**. [[CrossRef](#)]
28. Forsberg, R.; Tscherning, C.C. *An Overview Manual for the GRAVSOFTE Geodetic Gravity Field Modelling Programs*, 2nd ed.; 2008. Available online: https://www.academia.edu/9206363/An_overview_manual_for_the_GRAVSOFTE_Geodetic_Gravity_Field_Modelling_Programs (accessed on 17 May 2022).
29. Tscherning, C.C.; Rapp, R.H. *Closed Covariance Expressions for Gravity Anomalies, Geoid Undulations, and Deflections of the Vertical Implied by Anomaly Degree Variance Models*; Report No. 355; Dep. Geod. Sci. Ohio State University: Columbus, OH, USA, 1974.
30. Mayer-Gürr, T.; Behzadpur, S.; Ellmer, M.; Kvas, A.; Klinger, B.; Strasser, S.; Zehentner, N. ITSG-Grace2018—Monthly, Daily and Static Gravity Field Solutions from GRACE. *GFZ Data Serv.* **2018**. [[CrossRef](#)]
31. Vestøl, O.; Ågren, J.; Steffen, H.; Kierulf, H.; Tarasov, L. NKG2016LU—A new land uplift model for Fennoscandia and the Baltic Region. *J. Geod.* **2019**, *93*, 1759–1779. [[CrossRef](#)]